MODELLING OF A HYBRID ELECTRIC PROPULSION SYSTEM FOR SPACECRAFT

MODELISATION D'UN PROPULSEUR ELECTRIQUE HYBRIDE POUR VEHICULES SPATIAUX

A Thesis Submitted to the Division of Graduate Studies
of the Royal Military College of Canada
by

Alexander George Christou, B.A. Sc

Supervisor: Professor Manish Jugroot
Department of Mechanical and Aerospace Engineering

In Partial Fulfillment of the Requirements for the Degree of
Master of Applied Science in Aeronautical Engineering

April, 2015

© This thesis may be used within the Department of National Defence
but copyright for open publication remains the property of the author.

Abstract

Space technology is playing an ever-growing role in modern society. From communications systems to studying climate change and gravity waves, space is vital to furthering many fields of scientific and technical study. As the number and complexity of space missions grows, there is a critical need for efficient onboard thrusters. Electric propulsion presents an excellent alternative to conventional chemical rockets, with advantages for specific spacecraft applications. Hence, higher exhaust velocities from a plasma-based thruster allow for more efficient mass utilization and expanded mission capabilities. While there are several types of electric propulsion, two of the most currently utilized are Hall Effect thrusters and Ion thrusters. Each of these devices specializes in different mission types, due to their different operational modes. A hybrid Hall-ion thruster device is proposed to overcome the disadvantages (and enhance the advantages) of each thruster type. To investigate the proposed design, time-dependent multiphysics simulations were conducted to understand the detailed underlying phenomena. Plasma evolution within the thruster was studied and the presence of key trends was characterized. Parameters and design changes were studied in detail and thruster performance optimized based on results. The physical behaviour is in line with expectations from comparable electric thrusters for spacecraft.

Résumé

La technologie spatiale a des ramifications importantes dans le tissu de la société moderne. Elle contribue par exemple à l'étude du changement climatique et aux ondes gravitationnelles, et devient vital dans plusieurs domaines scientifiques et technologiques. Ainsi, quand le nombre et la complexité des missions spatiales augmente, la nécessité d'un système de propulsion efficace devient prépondérante. La propulsion électrique représente une alternative en comparaison à la propulsion traditionnelle de type chimique et possède des avantages pour certaines missions spécifiques de véhicules spatiaux. La vitesse d'éjection du carburant d'un propulseur ionique contribue à une efficacité accrue et des missions plus élaborées. Il existe plusieurs types de propulseurs électriques mais les deux couramment plus utilisées sont les propulseur ionique et de type Hall (chacun spécialisé pour des missions et des modes opérationnels spécifiques). Un propulseur hydride Ion-Hall est proposé afin de combiner les avantages (et limiter les inconvénients) de chaque type. Afin d'étudier le concept proposé, des simulations spatio-temporelles des espèces présents, visent la compréhension détaillée des phénomènes sous-jacents. L'évolution des particules chargées dans le propulseur a été étudiée et les zones et périodes clefs ont été caractérisées. La paramétrisation du propulseur a été étudiée et les conséquences ont été intégrées afin d'optimiser la performance. Le comportement physique est en accord avec les autres types de propulseur électriques pour véhicules spatiaux.

Contents

Abstract **ii**

Résumé **iii**

List of Tables **vii**

List of Figures **viii**

Nomenclature **xii**

1 Introduction to Electric Propulsion **1**
1.1 Rationale for Electric Propulsion for Space Missions 1
1.2 History of Electric Propulsion 5
1.3 Type of Thrusters 6
1.3.1 Ion thrusters 7
1.3.2 Hall Thrusters 10
1.4 Electric Propulsion Missions 12
1.5 Concluding Comments 15

2 Governing Equations and Modelling Theory **16**
2.1 Governing Equations 16
2.1.1 Fluid Equations 17
2.1.2 Plasma Equations 18
2.1.3 Source Terms 21
2.2 Simulation of Electric Propulsion Systems: Literature Review . 21
2.2.1 Ion Thruster Modelling 22
2.2.2 Hall Thruster Modelling 23
2.3 Simulation Conditions 24
2.3.1 Modelling: Multiphysics Approach 24
2.3.2 Model: Configuration and Key Parameters 25

2.4 Validation of Methods 26
2.4.1 Glow Discharge 27
2.4.2 Mesh Sensitivity Analysis 31
2.5 Concluding Remarks 33

3 Hybrid Electric Spacecraft Propulsion: Conceptual Design 34
3.1 Hybridization Considerations 34
3.1.1 Hybridizing the Magnetic Field 35
3.1.2 Hybridization of Electric Fields 37
3.2 Hybrid Thruster Concepts: Modelling 38
3.3 Hybrid Thruster Design: Components 42
3.3.1 Design Overview 42
3.3.2 Discharge Chamber 42
3.3.3 Hollow Cathode: Electron Source 43
3.3.4 Acceleration Channel 44
3.3.5 Magnetic Field 45
3.4 Hybrid Thruster Model Specifics 48
3.5 Concluding Remarks 50

4 Simulation and Hybrid Thruster Results 51
4.1 Introduction 51
4.2 Time Evolution 52
4.2.1 Initiation of the Discharge 52
4.2.2 Initiating Trends 54
4.2.3 Establishing Steady-State 56
4.2.4 Steady State 59
4.2.5 Ion Motion 66
4.3 Magnetic Field Optimization 68
4.3.1 Modified Magnetic Field 68
4.3.2 Magnetic Field Strength 73
4.4 Electric Potential Optimization 75
4.5 Thruster Performance 77
4.6 Concluding Remarks 79

5 Summary and Concluding Remarks 81
5.1 Conclusions 81
5.2 Future Considerations and Recommendations 84

Bibliography 86

Appendices **91**

A Appendix A **92**
A.1 Drift Diffusion Derivation 92

List of Tables

1.1 Performance information of two different chemical thrusters and an electric thruster (Hall type) are compared. Data from the European Space Agency. 5

4.1 Examples of Hall and ion thruster with specific impulse and thrust compared to the hybrid thruster. Note that the power of these thrusters ranges between 1-3 kW. 78

List of Figures

1.1 Flow diagram of and components of a liquid rocket system [1]. . . 2
1.2 Cross section of a solid-fuel rocket showing the propellant (grain), casing, and nozzle [1]. 3
1.3 Diagram of the interior of an RF ion thruster. Grey regions represent magnets. 8
1.4 Diagram of the interior of an DC ion thruster. Ring-cusp style magnetic field lines are shown. 9
1.5 Diagram of the interior of a Hall thruster. 11
1.6 NSTAR thruster, here shown on the Deep Space 1 probe. Source: NASA - (Great Images in NASA). 13
1.7 Artists illustration of GOCE, with the ion thruster and ion beam shown. Source: ESA - GOCE Mission. 14

2.1 Magnetic field strength in the ion thruster modelled by Wirz. A) Unmodified magnetic field. B) Magnetic field with increased central ring magnet strength. [2] 23
2.2 High speed video was used to capture time-lapse images of rotating spoke oscillations of ion number density. Contrast was enhanced using post processing techniques. Oscillations are visible as the brighter areas in the upper row, and the blue and red in the lower row. Brighter sections in the upper row (red in the lower row) represent regions of higher ion number density [3]. 26
2.3 Photograph of the different regions present within a glow discharge, with major regions labelled. Figure from Livoskiy et al [4]. 27
2.4 Electron density (m^{-3}) within the glow discharge simulation. . . . 29
2.5 Electric potential within the glow discharge simulation. 30

2.6 Electron number density in a glow discharge at a) 13 Pa, where the applied potential is 1) 350 V, 2) 400 V, 3) 500 V, 4) 600 V, and 5) 700 and b) 0.6 torr, where the applied potential is 1) 300 V, 2) 325 V, 3) 350 V, 4)375 V, 5) 400 V, and 6) 425 V [4]. 31
2.7 Electron density within the simulation using a mesh of (from left to right) 9000, 16000, and 32000 cells. 32
2.8 Comparison of electron density of the glow discharge along the axis for each mesh size. 33

3.1 Schematic of the hybrid thruster design tested, with key components and regions labelled. Dark grey regions represent magnets, hatched regions represent the anodes. 36
3.2 Front view of a potential support strut configuration for the hybrid thruster. 37
3.3 Cross sectional schematic of the NASA-173GT [5]. 39
3.4 Cross-section of the double-stage Hall thruster, with various components labelled [6]. 40
3.5 Schematic of the magnetic geometry with the HEMP thruster. . . 41
3.6 Schematic of a hollow cathode assembly, showing various components. 43
3.7 Acceleration channel of a Hall thruster with magnetic field lines shown, demonstrating the magnetic shielding technique of Conversano et al. [7] 45
3.8 Magnetic field lines within the hybrid thruster. 46
3.9 Schematic of a Hall thruster, with magnetic field lines also shown [8]. 47

4.1 Axisymmetric cross section of the hybrid thruster (see also Figure 3.1). Grey regions represent magnets. 52
4.2 Log of electron number density (m^{-3}) after 10 ns showing the effect of the hollow cathode. 53
4.3 Log of electron number density (m^{-3}) after 10 ns. 54
4.4 Log of electron number density (m^{-3}) after 100 ns. 55
4.5 Log of electron number density (m^{-3}) after 100 ns. Electrons ejected from the hollow cathode are accelerated towards the anode walls, concentrating along magnetic field lines. 56
4.6 Log of electron number density (m^{-3}) after 1 μs within the acceleration stage. Formation of a beam structure is being apparent. . . 57
4.7 Log of electron number density (m^{-3}) after 1 μs. Amplification of the electron number density within the discharge chamber is apparent. 58

4.8 Log of electron number density (m^{-3}) after 10 μs. Further amplification of the electron number density within the discharge chamber is visible. Confinement and a beam structure are forming through the acceleration section. 59
4.9 Log of electron density (m^{-3}) after 1 s. Steady-state of the system is reached. 60
4.10 Log of electron density (m^{-3}) at various times in the simulation, as found through the centre line of the acceleration stage. 61
4.11 Electric potential (V) within the thruster at 1 s. 62
4.12 Electron temperature (eV) after 1 s through the whole domain. . . 63
4.13 Electron temperature (eV) after 1 s in the discharge chamber. . . . 64
4.14 Electron temperature (eV) of the acceleration section. The high electric field through the acceleration section leads to substantially higher electron energies than are found throughout the rest of the domain. 65
4.15 Ionization rate ($m^{-3}s^{-1}$) within the thruster at 1 s. Highest ionization regions occur outside the hollow cathode, along magnetic field lines, and through the acceleration channel. 66
4.16 Ion velocity magnitude through the acceleration channel, with streamlines denoting flow. 67
4.17 Radial magnetic field strength (G) within the hybrid thruster after the addition of a second ring of magnets through the acceleration channel. 69
4.18 Radial magnetic field strength (G) within the hybrid thruster after the addition of a second ring of magnets through the acceleration channel. 70
4.19 Log of electron density (m^{-3}) after 1 s with an additional ring of magnets in the acceleration stage. 71
4.20 Electron density (m^{-3}) along the centreline of the acceleration stage after 1 s, as compared to the results for the unaltered magnetic field case. 72
4.21 Electron Temperature (eV) after 1 s for the altered magnetic field hybrid thruster. 73
4.22 Electron temperature for various magnetic field strengths, here denoted by the peak radial field strength for each case. A) 12 G B) 59 G C) 130 G D)180 G 74
4.23 Electron temperature within the acceleration stage after 1 s, for 4 different potentials. A) 245 V, B) 445 V, C) 745 V, D) 945 V. . . . 76
4.24 Ion density taken along a line through the centre of the acceleration stage for various discharge potentials. 77

5.1 Diagram of the hybrid thruster with key temporal moments and spatial locations noted. Blue denotes primarily electron dynamics, while orange represents ion dynamics. A) Hollow cathode ejects electrons into the discharge chamber, igniting the plasma. B) Reduced plasma density near walls due to impeded electron motion across field lines. C) Ions drift towards the acceleration stage. D) Ions flow into the acceleration channel, though particle flow is hindered by the addition of a an extra ring of magnets. E) Electrons along the exit plane reach high energies along the radial field lines due to high acceleration electric fields. F) Ions are ejected and accelerated by strong axial electric fields, forming the ion beam. . 83

Nomenclature

α_j	Townsend coefficient m^{-1}
B_x	Magnetic field, T
D_k	Mixture average diffusion coefficient, m^2/s
D_k^T	Thermal diffusion coefficient,$kg/m \cdot s$
$\overrightarrow{D_e}$	Electron diffusivity, m^2/s
$\overrightarrow{D_\epsilon}$	Electron energy diffusivity, m^2/s
$\overrightarrow{E}$	Electric field, V/m
E	Energy J
f_α	Boltzmann distribution function
$\frac{\partial f}{\partial t_{col}}$	Rate of change in distribution function due to collisions s^{-1}
F_α	Force on species α, N
g	Acceleration due to gravity $m/s/s$
$\overrightarrow{\Gamma_i}$	Particle flux, $m^{-2}s^{-1}$
$\overrightarrow{\Gamma_\epsilon}$	Energy flux, $m^{-2}s^{-1}$
H	Thrust N
I_{sp}	Specific impulse s
$\underline{I}$	Identity matrix
$\vec{j_k}$	Diffusive flux vector, $kg/m^2 \cdot s$
k_B	Boltzmann constant J/K
m_α	Mass of species α, kg
m_0	Initial mass of the spacecraft kg
m_1	Final mass of the spacecraft kg
m_i	Mass of particle, i kg
$\dot{m}$	Mass flow rate, kg/s
M_n	Mean molar mass, kg/mol
$\overrightarrow{\Gamma_e}$	Electron flux, $m^{-2}s^{-1}$
μ_k	Mixture average mobility of species k, $m^2/V \cdot s$
μ_{dc}	Electron mobility in the absence of a magnetic field, $m^2/V \cdot s$
$\underline{\mu_e}$	Electron mobility, $m^2/V \cdot s$

$\underline{\mu_\epsilon}$	Electron energy mobility $m^2/V \cdot s$
$\mu_{e,\perp}$	Cross field electron mobility $m^2/V \cdot s$
Ω_e	Hall parameter
ω_k	Mass fraction of species k
R_k	Neutral number density, m^{-3}
n_i	Particle number density, m^{-3}
ν_m	Momentum collision frequency s^{-1}
ν_j	Collision frequency for reaction j, s^{-1}
n_ϵ	Electron energy density V/m^3
p	Pressure Pa
$\underline{p_i}$	Pressure Pa
q_i	Charge on particle i Pa
ρ	Initial mass of the spacecraft kg/m^{-3}
R_i	Reaction rate, $m^{-3}s^{-1}$
R_e	Electron rate expression, $m^{-3}s^{-1}$
R_k	Rate expression, $kg/m^3 \cdot s$
σ_j	Cross section of reaction j, m^2
t	time, s
T	Temperature, K
$\overrightarrow{v}$	Velocity, m/s
v_e	Exhaust velocity m/s
ΔV	Change is spacecraft velocity m/s
$\overrightarrow{V_k}$	Diffusive velocity, m/s
x_j	Species weight fraction
z_k	Charge of species k

1 Introduction to Electric Propulsion

1.1 Rationale for Electric Propulsion for Space Missions

There are many varieties of spacecraft propulsion to fit the wide range of mission requirements. The most common type of spacecraft propulsion are immense chemical rockets used to lift material from Earth into space. Currently, the only viable way to reach space is through the use of exothermic chemical reactions. High pressure ejects material out of the rocket, and due to conservation of momentum, the rocket is accelerated in the opposite direction. This type of rocket is commonly referred to as chemical propulsion, as it makes use of potential chemical energy to achieve thrust. Within the class of chemical propulsion, two main categories are defined: solid-fuel propulsion and liquid-fuel propulsion. Each form of chemical propulsion offers its own advantages and so are used for particular purposes.

Solid propellant offers a stable and reliable way to create thrust. As such, it is often used for missiles and model rockets. Modern liquid propellants have greater performance than solid rockets, but come with additional issues due to increased complexity. A liquid rocket requires pumps and machinery to properly feed fuel into the reaction (see Figure 1.1). Additionally, cryogenic temperatures may be required to store the liquid propellants (such as liquid oxygen or liquid hydrogen). This makes liquid propellant systems more expensive and riskier to operate. In addition to better raw performance, liquid-fuel also provides increased flexibility compared to solid fuel. In contrast, solid propellant is burned where in the same place it is stored, as shown in Figure 1.2.

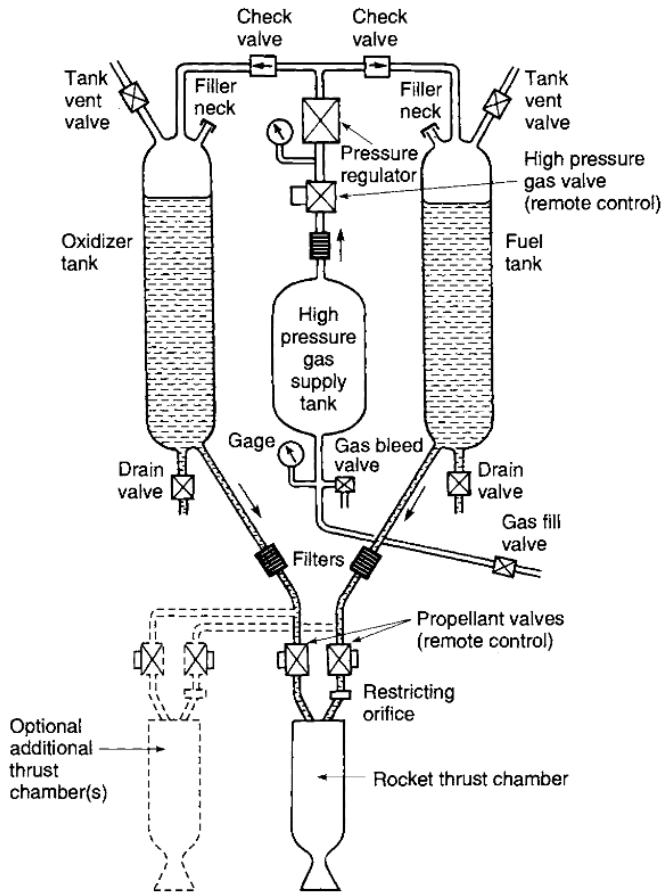

Figure 1.1: Flow diagram of and components of a liquid rocket system [1].

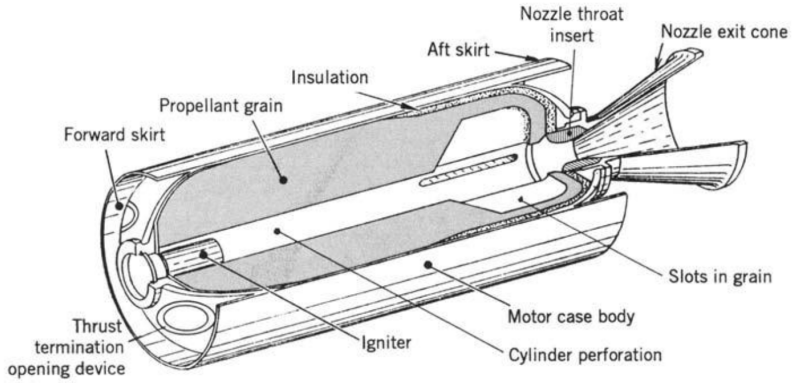

Figure 1.2: Cross section of a solid-fuel rocket showing the propellant (grain), casing, and nozzle [1].

In a liquid rocket, the fuel is supplied by pumps from tanks, and may be turned on and off as required. Additionally, controlling the mass flow allows for the thrust to be easily controlled in a liquid system. Active thrust control in a solid-fuel rocket is impossible, though the size of the surface exposed to the reaction may be changed to create different thrust profiles. Additionally, solid and liquid systems can be combined by feeding a liquid fuel into the solid fuel reaction chamber. This allows for some control over the rocket thrust, while taking advantage of the simplicity of solid rocket systems.

Both types of chemical propulsion are able to generate tremendous thrust. However, the impulse produced per unit mass of propellant, or specific impulse (see Equation 1.2), is relatively low compared to other propulsion technologies. A higher specific impulse implies that a lower flow rate of fuel is required to achieve the same thrust. Equivalently, less fuel is required at a higher specific impulse to generate the same change in momentum over the same amount of time. So, while chemical rockets are capable of immense thrust (10 000 kN in some cases) and momentum changes, they do so at the cost of burning large quantities of fuel. This makes them well suited to putting objects into space, but less ideal for use once in space, as large amounts of fuel would need to be on hand. Further, in the case of solid rockets, the rocket cannot be throttled, which greatly limits control and flexability.

Electric propulsion (EP) is in many ways complementary to chemical propulsion. While the thrust of a chemical rocket is can be large, the thrust generated by EP is extremely low, often in the range of 1 mN (colloid thruster) to 5 N (Variable Specific Imupulse Magnetoplasma Rocket, in development).

This minuscule thrust makes lifting objects into space using EP impossible for long into the foreseeable future. However, EP systems produce high specific impulses compared to chemical thrusters. This allows EP to expand space mission capabilities. Specifically, EP systems attain exhaust velocities in excess of 20 km/s, compared to the exhaust velocities of traditional chemical propulsion at 4 km/s [1]. Thrusters which produce high exhaust velocities are of interest as they allow the spacecraft to more efficiently utilize propellant. This fact is expressed by examining the specific impulse of a propulsion device, which translates the thrust generated per unit mass of propellant, per unit time. Equivalently, EP systems can achieve larger changes in spacecraft velocity using comparable amounts of propellant. This is seen through the Tsiolkovsky Rocket Equation (Equation 1.1) [9]. The Rocket Equation as presented here is written excluding gravity and the thrust due to pressure, as this is insignificant for EP.

$$\Delta V = v_e ln\left(\frac{m_0}{m_1}\right) \tag{1.1}$$

The rocket equation shows that the overall change in velocity of a spacecraft (in the absence of external forces), ΔV, is based on the exhaust velocity of the propellant, v_e, and the natural logarithm of the initial and final spacecraft mass. EP devices generate changes in space velocity by creating a high exhaust velocity and a relatively small mass ratio. Chemical systems have a comparatively small exhaust velocity, but a much larger mass ratio. Higher exhaust velocities imply greater propellant mass efficiency for a propulsion system. The effect of exhaust velocity on performance is quantified through a term called the specific impulse, the definition of which is shown in Equation 1.2. Specific impulse is the change in momentum produced per unit mass (or weight) of propellant. Often specific impulse is calculated per unit weight, giving it units of seconds. In Table 1.1, propulsion systems from different missions are compared. Note that the monopropellant shown has lower thrust than a comparably sized bipropellant as it is fueled by an exothermic decomposition reaction, rather than combustion.

$$I_{sp} = \frac{F_{Thrust}}{\dot{m}g} \tag{1.2}$$

Table 1.1: Performance information of two different chemical thrusters and an electric thruster (Hall type) are compared. Data from the European Space Agency.

	Monopropellant Thruster	**Fregat Main Engine**	**SMART-1 Hall Thruster**
Propellant	Hydrazine	Nitrogen tetroxide/ Dimethtylhydrazine	Xenon
Specific Impulse (s)	200	320	1640
Thrust (N)	1	1.96×10^{4}	6.8×10^{-2}
Thrust time (h)	46	0.24	5000
Propellant (kg)	52	5350	80
Total impulse (Ns)	1.1×10^{5}	1.72×10^{7}	1.2×10^{6}

Using a similar amount of propellant to the small monopropellant thruster the Hall thruster creates a total impulse an order of magnitude greater. Equivalently, the thruster achieves 10% of the total impulse created by the larger hydrazine thruster, using only 1.5% of the fuel.

Additionally, as the name suggests, EP derives its energy from electrical power. This provides great benefit in terms of mission longevity as solar panels may then be used to produce the required energy, provided the mission is in the vicinity of the sun. However, satellites and spacecraft often operate with relatively low power, on the order of a few kilowatts, limiting the size of the EP device used. The power systems required by EP are sometimes large and complex, though even including the mass of the power systems, EP is generally more mass efficient than conventional chemical propulsion.

1.2 History of Electric Propulsion

EP technology has undergone a long journey from a dream of early visionaries to a growing space technology. Originally envisioned to aid in human exploration of the planets, electric propulsion (EP) remained a technological curiosity for most of the time since it was proposed. After many years of design, it now plays a role on hundreds of spacecraft. The advantages of EP over chemical systems will allow it to be an attractive technology for many years into the future.

EP was originally proposed by one of the founders of rocketry, Konstantin Tsiolkovsky [10]. The idea likely came to Tsiolkovsky from a popular topic in physics at the time, the cathode ray tube (CRT). Within the CRT, electrons

are accelerated to tens of thousands of kilometres per second. Recognizing the importance of high velocity particles for rocketry (See Rocket Equation, Eqn 1.1), Tsiolkovsky foresaw that electric forces may hold potential advantages over chemical propulsion. Discoveries in atomic physics, such as the ion opened the door for further EP investigation. Tsiolkovsky quickly recognized the greater mass of the ion as more useful than that of electrons for propulsive purposes. Quite ahead of his time, Tsiolkovsky wrote, "The force of electricity is unlimited and can, therefore, produce a powerful flux of ionized helium to serve a spaceship. However, we shall leave these dreams for a while and return to our prosaic explosives." [10].

Early in the 20th century, another visionary, Robert Goddard, applied developing modern physics to practical study of electrical propulsion. During his study of EP, he realized that ejecting a stream of charged particles will result in a build-up of charge on the spacecraft. To counteract this, the particles stream ejected must be neutral in charge. This remains an important consideration for modern electrical propulsion. In 1917, Goddard would go on to produce what would be recognized as the first electrostatic ion accelerator for propulsion purposes [10].

Further work was done in EP by Yuri V. Kondratyuk. Kondratyuk is noted as having given the first suggestions of what would eventually become colloid thrusters, using more massive liquid droplets in place of individual ions. Additionally, Kondratyuk noted that practical synergy of using EP along side solar panels on spacecraft. Like Tsiolkovsky and Goddard, Kondratyuk believed that, while EP held great potential, chemical propulsion was likely to be more practical for the immediate future. Chemical propulsion system can generate thrust in the range of thousands of kilonewtons, capable of lifting mass into orbit (or beyond) from the Earth's surface. However, as shown by the lower specific impulse, chemical rockets use large amounts of fuel to generate that thrust. This prevents them from being particularly effective in space missions requiring large changes in velocity. While chemical thrusters are theoretically capable of many high velocity space missions, the mass of fuel required becomes prohibitively high, or, equivalently, the payload capacity becomes prohibitively low.

1.3 Type of Thrusters

A large variety of EP devices are being researched and used today. They are generally divided into 3 categories: electrothermal, electromagnetic, and electrostatic. Electrothermal, as the name implies, use electric currents to heat a

propellant gas to high temperatures and pressures, expanding this gas to generate thrust. A common type of electrothermal device is the arcjet, utilizing an electric arc to heat the propellant [11]. Electromagnetic devices utilize a combination of electric and magnetic fields to accelerate the propellant, such as found in magnetoplasmadynamic thrusters [12]. Lastly, electrostatic devices accelerate the propellant using a static electric field. Ion thrusters and Hall-effect thrusters (often simplified to Hall thrusters) are examples of electrostatic thruster [13, 14]. It should be noted that Hall thrusters do make use of magnetic fields to ionize the propellant, however, the acceleration of the propellant is achieved through purely electrostatic means.

1.3.1 Ion thrusters

Though many types of electrostatic devices exist, the most prevalent are the ion thruster and Hall thruster. An ion thruster begins by sending neutral gas (the propellant) into a plasma discharge chamber. The propellant gas is ionized inside the discharge chamber, with the particular ionization method depending on the type of thruster. Popular methods of ionizing the neutral gas are through radio-frequency (RF) induction currents or direct current (DC) discharge [15, 2]. In the case of RF ionization, a set of coils around the discharge chamber create an axial, sinusoidally varying magnetic field. The axial RF magnetic field in turn generates an RF azimuthal electric field. Free electrons are driven by the electric field in an azimuthal current, colliding with and ionizing neutral gas atoms. Figure 1.3 shows a diagram of the RF-thruster components.

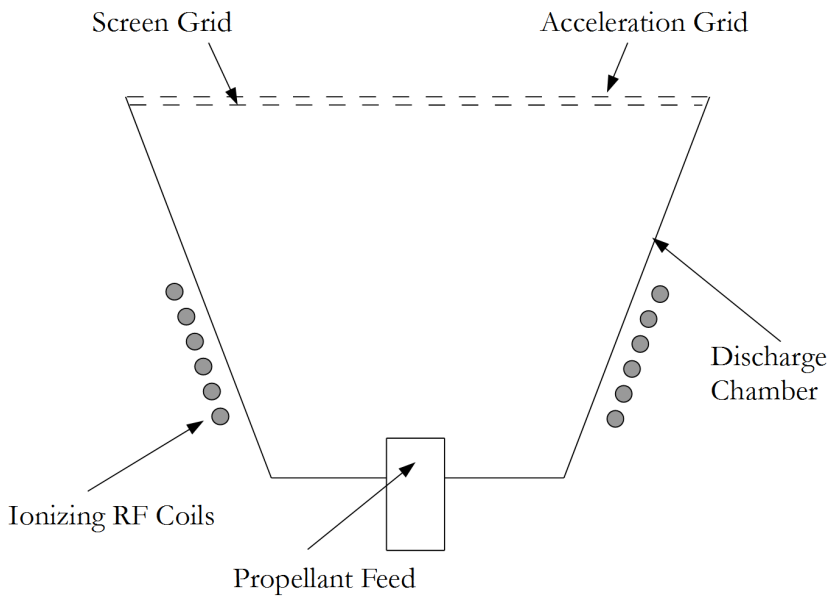

Figure 1.3: Diagram of the interior of an RF ion thruster. Grey regions represent magnets.

A DC-style ionization stage (Figure 1.4), of particular interest in this paper, uses a hollow cathode to generate a stream of electrons. These are then injected into the discharge chamber. The electrons are accelerated by an electric field, increasing in energy and causing ionization through collisions with neutral gas atoms. Additionally, a magnetic field is established inside the discharge chamber in order to increase the probability of a collision between electrons and neutral atoms. Electrons in a magnetic field will follow spiral paths, increasing their path length inside the discharge. Additionally, a properly shaped magnetic field inside the discharge chamber reduces electron losses to the walls, as electrons have greatly reduced mobility across magnetic fields.

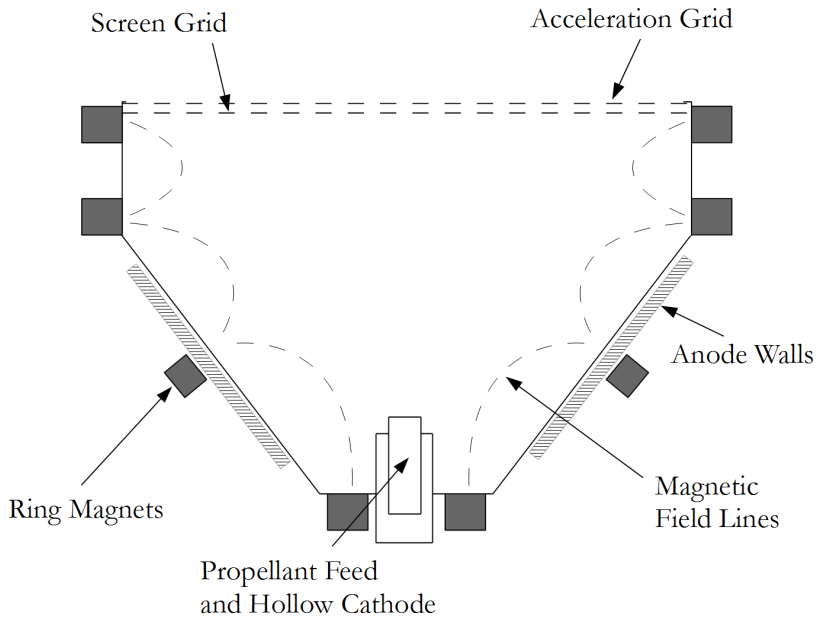

Figure 1.4: Diagram of the interior of an DC ion thruster. Ring-cusp style magnetic field lines are shown.

The ions within an ion thruster are then accelerated through the use of a series of electrodes called grids. Generally, two grids are used, though three or more are not uncommon [16]. The first grid, in contact with the plasma discharge, is called the screen grid. This is an electrode which is set to the potential of the cathode, often up to 1000 V. The screen grid also has a series of small holes drilled in it to allow ions to be drawn out of the plasma. This grid maintains a sheath in contact with the discharge, preventing electrons from leaving the plasma. Directly behind the screen grid is an electrode set to a negative potential relative to the spacecraft ground (in the realm of -150 V), again with small holes drilled in it. This second grid electrode is named the acceleration grid. Ions are extracted and accelerated by the negative potential, producing thrust. External to the thruster is a second hollow cathode, which injects electrons into the ion exhaust, maintaining zero charge on the spacecraft and preventing a voltage build-up outside the thruster from stalling the beam.

Ion thrusters are able to achieve efficient operation, in the realm of 50-70%. High exhaust velocities are achieved by the large potential drop the ions experience as they travel from the plasma past the acceleration grid. However,

because only the positively charged ions are extracted from the plasma, there is a limit on the power density of the thruster. Upon gradually increasing the potential difference between the screen and acceleration grids, the ion beam current will eventually reach a saturation point. This imposes a limit on the total thrust and power which a specific ion thruster may produce.

Additionally, the grids used by ion thrusters are subject to potential sputtering due to the ion flux generated. Specifically, the erosion effect is largely due to the doubly ionized gas atoms, which follow different trajectories as they are accelerated, and hence cannot be guided smoothly through the screen and acceleration grids [17]. This means that grid erosion is a large concern in the application of ion thrusters to long term space missions.

1.3.2 Hall Thrusters

The second type of commonly used electrostatic thruster is the Hall thruster. A Hall thruster adopts a very different geometry and method of ionizing propellant. Figure 1.5 shows a cross-section of a typical Hall thruster. In place of the cylindrical discharge chamber used in most ion thrusters, the discharge chamber in a hall thruster is a circular channel. One side of the channel is open to space, the other side is covered by an anode. In conjunction with a neutralizing cathode outside the thruster, the anode generates an axial electric field, used to accelerate the ionized propellant. A radial magnetic field is generated across the channel by a set of magnets located in the core and around the discharge channel. The axial electric field and the radial magnetic field generate a Hall current of electrons, which drift azimuthally around the chamber, ionizing neutral gas particles along their path. The axial electric field then accelerates the ions, generating the spacecraft's thrust. As with an ion thruster, the ion beam must be neutralized to prevent the build-up of charge on the spacecraft. An external hollow cathode is commonly used. In a Hall thruster, the external Hollow Cathode also provides seed electrons to help the ignition of the Hall thruster. Electrons are drawn into the discharge channel by the axial electric field, where they begin to travel azimuthally, colliding with and ionizing neutral propellant atoms.

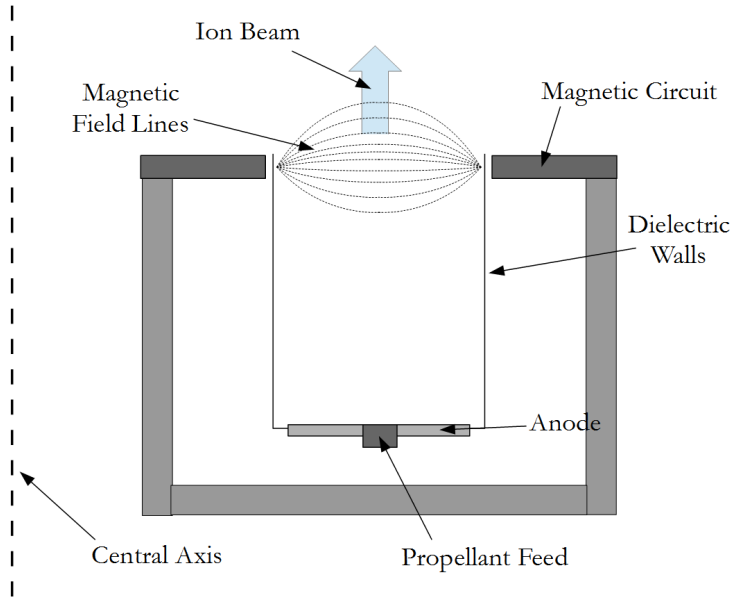

Figure 1.5: Diagram of the interior of a Hall thruster.

Compared to an ion thruster, the specific impulse of a Hall thruster is generally lower due to the lower acceleration potentials used. While ion thruster often reach 1100 V discharge potentials, Hall thrusters generally operate at 300-500 V. At higher potentials, discharge losses in Hall thrusters increase to prohibitively high levels. However, the total thrust of a Hall thruster is often higher than comparable ion thrusters. The cause of this disparity is due to what is termed space-charge limitations. The purely positive space-charge in the grid region eventually generates a potential which counteracts the applied potential. This means that the amount of current flowing through the grids is saturated, and increases in acceleration potential will not increase the thrust that the ion thruster generates. In Hall thrusters, the ions are accelerated from a region of quasi-neutrality, as there are electrons and ions in nearly equal proportion within the discharge channel. This removes any space charge limitations on the thrust of the Hall thruster. Space-charge limitations are met in ion thrusters as they must accelerate ions through a plasma sheath. The plasma sheath forms due to surface charge accumulation on the screen electrode, as electrons build-up on its surface quicker than ions. Within an ion thruster, electrons have a much greater temperature than ions. This allows them to leave the plasma at a much greater rate, leading to electron accumula-

tion along the walls. The electrons attract ions and repel electrons. While this sheath is crucial to the charge confinement of electrons within the discharge chamber, it has the side effect of creating a region of purely positive space charge. The space charge counteracts the effect of an applied acceleration potential, leading to thrust saturation. Without the space-charge limitations, higher power and thrust is often achievable in a Hall thruster [18].

Given that Hall and ion thrusters each have specific advantages and drawbacks, this work explores whether it is possible to create a hybrid thruster able to achieve performance greater than each pure thruster type.

Previous work has been conducted in a similar vein by Peterson [5]. Peterson coupled the ionization stage of an ion thruster with a single stage Hall thruster to reduce the losses which occur in Hall thrusters at high discharge potentials. Specifically, increase the propellant utilization beyond that of a Hall thruster by adding an additional ionization stage and decrease the generation of doubly ionized propellant atoms. A Hall thruster begins to generate large amounts of doubly ionized atoms at higher discharge potentials. These doubly charged ions are a significant source of erosion and efficiency loss within the thruster. The Hall thruster is optimized to direct singly charged ions into the exhaust plume without colliding with the discharge channel walls. Doubly charged ions experience extra electromagnetic forces, and so are much more likely to collide with walls and cause sputtering.

1.4 Electric Propulsion Missions

Hall and ion thrusters have been discussed and researched for almost a century, though they remained impractical for many reasons. An EP device requires a fairly large power supply and more advanced electronic systems than a conventional cold gas thruster. However, recent advances in power system and solar technology aboard satellites have opened up the potential for EP devices to be used on all sorts of satellites and space science missions. Additionally, there is a technologically conservative attitude in the spacecraft industry, making the entry of new and largely untested technologies rather difficult. Space flight is an expensive endeavour, so some reticence of new technology is to be expected. Currently, EP has been used on more than 200 spacecraft [10]. Growth in EP applications will likely to continue as the technology becomes more mature and trusted.

In order to better understand the application of EP devices a review of an actual mission may prove useful. One of the most important milestones in EP came with the launch of the Deep Space 1 mission, and the use of an ion

thruster as its primary propulsion system [19]. The Deep Space 1 mission was originally to do a flyby of an asteroid, however, the mission was later extended to include a flyby of a comet. An ion thruster, called the NASA Solar electric propulsion Application Technology Readiness (NSTAR) project (Figure 1.6), was used to generate a ΔV of 4.5 km/s and propel the spacecraft on its orbit. The NSTAR performance exceeded expectations, and served as a validation of EP technology for deep-space applications. To illustrate the benefits of using EP, consider the ESA's Rosetta mission. Rosetta used chemical propulsion to reach a comet. It had an initial mass of 2900 kg, final mass of 1300 kg, and took 9 years to reach the comet. An ion thruster system would have had an initial mass of 1830 kg, final mass of 1300 kg, and taken 2.5 year to reach the comet. Additionally, the ion thruster would allow a sample to be returned to the Earth [13]. The differences in initial masses are significant enough that smaller and cheaper launch vehicles may be used, greatly reducing costs. With the successful validation test of the NSTAR on Deep Space 1, missions designers EP can bring great benefits to deep space missions.

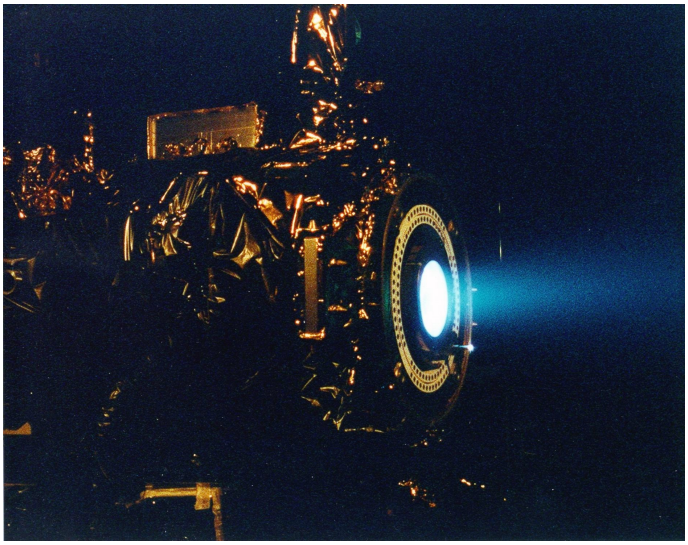

Figure 1.6: NSTAR thruster, here shown on the Deep Space 1 probe. Source: NASA - (Great Images in NASA).

Another example of a mission which made use of EP technology is the ESA's Gravity Field and Steady-State Ocean Circulation Explorer (GOCE) [20]. A picture of GOCE can be see in Figure 1.7. The purpose of the GOCE mission was to map the Earth's gravity field in great detail, giving new information

about the interaction of gravity and the oceans' currents. The mission flew at a fairly low orbit of 255 km in order to get more accurate readings from its accelerometers [21]. An ion thruster was used on the mission to maintain its orbit and counteract the effects of drag which heavily impede motion at such a low altitude. Additionally, an ion thruster produces far less vibration than a chemical thruster, and so did not affect the sensitive gyroscopes required for gravity measurements. The ion thruster remained in operation for 55 months, though the initial mission was planned for only 20 months. Low solar activity during the operating period meant the upper atmosphere was calmer than normal, and hence less drag.

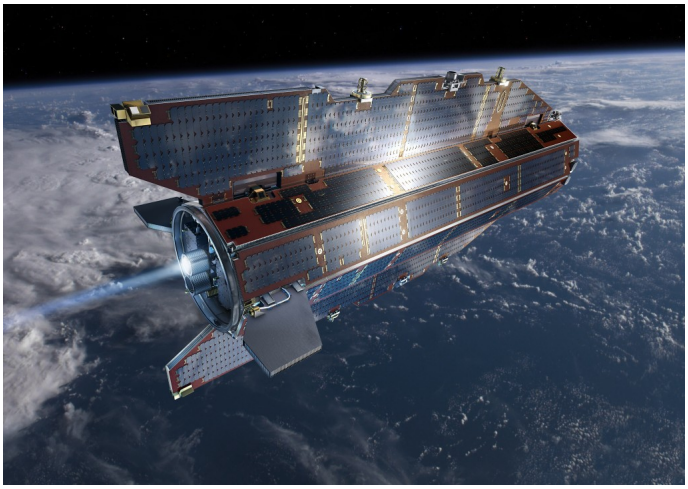

Figure 1.7: Artists illustration of GOCE, with the ion thruster and ion beam shown. Source: ESA - GOCE Mission.

In addition to the ion thrusters, Hall thrusters have been used for a variety of missions. The high specific impulse of ion thrusters mean they are ideal for long duration missions, as they will produce greater velocity changes for a given propellant mass. However, for shorter missions requiring greater thrust, such as orbit transfers, a Hall thruster is often ideal. One such mission is the ESA's Small Missions for Advanced Research in Technology-1 (SMART-1) [22]. This mission was designed to orbit and study the moon. SMART-1 began in an orbit around the Earth, then gradually spiralled outward to higher altitudes due to the thrust of the Snecma PPS-1350-G, a 1.3 kW Hall thrust. The thruster operated for 5000 hours, producing a total ΔV of 3.9 km/s [13].

Hall and ion thrusters have complimentary attributes. Ion thrusters are often able to function more efficiently, but are limited in their total thruster.

Comparatively, a Hall thruster can be more easily scaled to produce greater thruster. An investigation is conducted to determine if different features of Hall and ion thrusters could be combined to produce a hybrid thruster with better performance than each thruster type separately. The hybrid thruster should be able to attain higher specific impulse than a Hall thruster as well as higher specific impulse than an ion thruster.

1.5 Concluding Comments

EP systems offer advantages over traditional chemical propulsion for specific space missions. The low thrust and high specific impulse of EP thrusters makes them ideal for long duration, high ΔV missions. Missions costs can be reduced due to the mass saved by using a propulsion system with a higher specific impulse. However, the utilization of electrical energy means the thruster requires a kilowatt or larger power source, adding complexity to the spacecraft design. Hall and ion thrusters are electrostatic EP devices that have complementary performance traits. Hence, the objective of this work is to model a hybrid Hall-ion thruster with the aim of improved performance based on the advantages of each component thruster type. A hybrid thruster design will be proposed and modelled in order to test the concepts potential and understand underlying phenomena.

2 Governing Equations and Modelling Theory

Modelling of electric propulsion (EP) devices is crucial to the design process. EP devices are complex and expensive to test as they require large vacuum facilities. Time within these vacuum facilities is in high demand, and so much of the design process must be guided by analytic techniques and, more recently, advanced modelling efforts. As discussed earlier, there is a wide range of EP devices. Each of these devices operates with a different type of plasma, and so require different modelling techniques. The main equations used for plasma modelling will be discussed. The equations defined will have the capability of modelling the space and time evolution of the plasma within the electric thruster. Additionally, some notable EP modelling efforts will be introduced and discussed.

2.1 Governing Equations

Plasma is often deemed the fourth state of matter. While exciting, this statement does not provide any particularly enlightening information. Plasma is indeed different from standard matter, though it is disingenuous to say that it is just as similar to a solid as a gas. Some clarification is needed at this point in regards to the type of plasma being discussed. The revolution in solid-state physics brought to light that electrons, holes, and quasi-particles within a semiconductor could be thought of as forming a plasma. However, this thesis will focus on gaseous plasma, though often similar equations and terminology may be used to describe both semiconductor and gaseous plasma. As with a gas, a plasma is made of a collection of molecules, atoms, and electrons which are free to move relative to each other. However, while in a conventional fluid the particles influence each other only through collisions, particles in a plasma may exert electromagnetic forces on each other due to their non-zero charge.

An additional complication is that collisions in a plasma can create or remove particles by ionization or recombination reactions. An electron colliding with a neutral particle can knock off valence electrons, changing the neutral particle into an ion and an electron (see Section 3.4). Additionally, an electron may collide with and be reattached to an ion, forming a neutral particle. A useful exercise is to outline the ways in which plasma is different or similar to more conventional fluids.

2.1.1 Fluid Equations

A fluid may be described through the use of conservation equations. Equations 2.1, 2.2, and 2.3 represent fluid conservation equations for mass, momentum, and energy. The equations shown here (Euler equations) describe inviscid flow, a more fundamental description of fluids is given by the Navier-Stokes equations.

$$\frac{\partial \rho}{\partial t} + \nabla \cdot (\rho \overrightarrow{v}) = 0 \tag{2.1}$$

$$\frac{\partial (\rho \overrightarrow{v})}{\partial t} + \nabla \cdot (\rho \overrightarrow{v} \overrightarrow{v}^T)) = \rho g - \nabla p \tag{2.2}$$

$$\frac{\partial E}{\partial t} + \nabla \cdot (\overrightarrow{v}(E + p)) = 0 \tag{2.3}$$

The three equations from the conservation of momentum produce five equations with six unknowns, requiring an equation of state for closure. An important difference between plasma and fluids is the multiple constituents within a plasma. A fluid can often be considered as made of a single component, though the make-up of the fluid may actually be a mixture (as with the oxygen and nitrogen mixture making up air). In a plasma, the different species within may act differently (different velocity, directions, lifetimes), and so a separate set of equations must be used to describe each. For example, neutral atoms will not experience forces due to electromagnetic fields, and so will not interact in the same ways with electrons as ions. Additionally, a plasma is a continuous reaction, where species are able to change and produce other species. This means that conservation of mass, while still required, must be expanded to include the fact that particles may change into each other. Further, charge is a quantity which can flow within the plasma, and this must also be conserved. To account for the electromagnetic considerations, one must include Maxwell's Equations to be solved simultaneously with the fluid equations. Combined, fluid equations and Maxwell's equations form

Magnetohydrodynamic (MHD) equations. MHDs are widely applicable, and may be used to model systems ranging from fusion reactors to electrolyte flow in a liquid. Often, the full MHD equations are not necessary, and simplified systems may be used.

In the modelling undertaken here, the gas flow is assumed to be laminar, adiabatic, and inviscid. The neutral gas is not driven by any pressure or velocity differences on the boundary conditions, and so turbulent flow is not considered, but plasma turbulence may be important in certain localized regions. Mass flow of neutral particles is driven by diffusion, as there are no pressure differences. The transport of heavy species (including the neutral gas) is described by Equation 2.14, in the following section.

2.1.2 Plasma Equations

Plasma equations are often derived from a fundamental thermodynamic description of the system. Particle transport within a plasma is governed by the Boltzmann Transport Equation (BTE) shown in Equation 2.4. The BTE is a fundamental equation describing the state of a system of a large number of particles which are not in thermodynamic equilibrium. The state of the system is described by a distribution function, f, which provides the number of particles in a system having a given position and velocity. Solving the BTE is a challenging and computationally expensive endeavour due to its integro-differential and 6-dimensional nature (three position and three velocity components), as well as the complexity of the RHS collision term. The collisional term will be discussed later in Section 2.1.3.

$$\frac{\partial f_\alpha}{\partial t} + \vec{v} \cdot \nabla_r f_\alpha + \frac{\vec{F_\alpha}}{m_\alpha} \cdot \nabla_v f_\alpha = \frac{\partial f}{\partial t}_{col} \tag{2.4}$$

Instead of directly solving the BTE, a set of conservation equations is obtained from the BTE by taking the first three moments about it. The resulting three moments yield fluid conservation equations in density, energy, and momentum. These are shown in Equations 2.5 to 2.7.

$$\frac{\partial n_i}{\partial t} + \nabla \cdot \overrightarrow{\Gamma_i} = R_i \tag{2.5}$$

$$\frac{\partial}{\partial t}(n_i m_i u_i) + \nabla \cdot n_i m_i \overrightarrow{u_i} \overrightarrow{u_i^T} = -(\nabla \cdot \underline{p_i}) + q_i n_i \overrightarrow{E} - n_i m_i \overrightarrow{u_e} \nu_m \tag{2.6}$$

$$\frac{\partial n_\epsilon}{\partial t} + \nabla \cdot \Gamma_\epsilon + \overrightarrow{E} \cdot \Gamma_i = R_\epsilon \tag{2.7}$$

The conservation equations must be solved for each species in the plasma. This quickly becomes prohibitively complex to solve, and so the drift-diffusion approximation is used. The drift-diffusion approximation reduces the number of partial differential equations solved by introducing a term for the particle flux, Γ_i. Particle flux is derived from the momentum conversation, Equation 2.6, assuming the momentum collision frequency is much greater than the ionization and attachment frequencies. If the particles follow a Maxwellian energy distribution, the pressure term may be replaced as shown in Equation 2.8.

$$\underline{p_i} = n_i k_B T_i \underline{I} \tag{2.8}$$

The mobility, μ_i and the diffusion D_i are calculated and input into the plasma model. This approximation is valid so long as the mean free path between electrons and background gas is less than the characteristic length scale of the model and the thermal velocity is less than the electron drift velocity - in other words, the plasma must be collisional. In the future, the limits imposed by the drift-diffusion assumption at low pressures could be complemented by a particle code (for example a DSMC or PIC code), but would come at the expense of design and iteration flexibility [23]. Interestingly, Hall thruster models have successfully used the drift-diffusion approximation for modelling the electrons. The mean free path length of electrons within a Hall thruster is generally longer than the channel width of a Hall thruster. However, because the electrons mostly drift around in the azimuthal direction, they do not collide with the channel walls often - implying that for electrons, the plasma can be considered collisional [24].

A multiphysics software (COMSOL), combining the dynamics of the plasma, propellant, electric field, and magnetic field, was used in order to couple the different phenomena. A plasma is the combination of product of many different realms of physics, and as such proper coupling between variables is crucial. The simulations conducted here incorporate coupling between electron, ion, and neutral particles. An axisymmetric configuration was used to model the ion thruster and the hybrid version of the thruster. The equations used for modelling electrons dynamics are summarized in Equations 2.9 to 2.12.

$$\frac{\partial n_e}{\partial t} + \nabla \cdot \vec{\Gamma_e} = R_e - (\vec{v} \cdot \nabla) n_e \tag{2.9}$$

$$\vec{\Gamma_e} = -(\underline{\mu_e} \cdot \vec{E}) n_e - \vec{D_e} \cdot \nabla n_e \tag{2.10}$$

$$\frac{\partial n_\epsilon}{\partial t} + \nabla \cdot \vec{\Gamma_\epsilon} = R_\epsilon - (\vec{v} \cdot \nabla) n_\epsilon \tag{2.11}$$

$$\overrightarrow{\Gamma_\epsilon} = -(\underline{\mu_\epsilon} \cdot \overrightarrow{E})n_\epsilon - \overrightarrow{D_\epsilon} \cdot \nabla n_\epsilon \tag{2.12}$$

The inclusion of magnetic field effects is accomplished by using the tensor form of the electron mobility shown in Equation 2.13. The inverse of the electron mobility tensor is shown, as mobility itself cannot be written in a concise form. This form of the magnetic mobility tensor includes the effects of $\overrightarrow{E} \times \overrightarrow{B}$ drift as well as the effects of reduced mobility across field lines.

$$\underline{\mu_e^{-1}} = \begin{bmatrix} \frac{1}{\mu_{dc}} & -B_z & B_y \\ B_z & \frac{1}{\mu_{dc}} & -B_x \\ -B_y & B_x & \frac{1}{\mu_{dc}} \end{bmatrix} \tag{2.13}$$

For the non-electron species, diffusion equations were used, namely the continuity equation shown in Equation 2.14. The diffusive flux vector is defined as shown in Equation 2.15. Using a Mixture Averaged assumption, the diffusion velocity for each species is defined as shown in Equation 2.16.

$$\rho \frac{\partial}{\partial t}(\omega_k) + \rho(\overrightarrow{u} \cdot \nabla)\omega_k = \nabla \cdot \overrightarrow{j}_k + R_k \tag{2.14}$$

$$\overrightarrow{j_k} = \rho \omega_k \overrightarrow{V_k} \tag{2.15}$$

$$\overrightarrow{V_k} = D_k \frac{\nabla \omega_k}{\omega_k} + D_k \frac{\nabla M_n}{M_n} + \frac{D_k^T}{\rho \omega_k} \frac{\nabla T}{T} - z_k \mu_k \overrightarrow{E} \tag{2.16}$$

The mixture-averaged formulation is a simplification of the full Maxwell-Stefan equations. As with the Maxwell-Stefan equations, this formulation preserves mass conservation within the system with the benefit of being much less computationally expensive than the full Maxwell-Stefan equations. The computational ease (and loss of accuracy) is a result of using a simplified expression for the diffusion coefficient, D_k.

It is interesting to note that the plasma model makes use of the drift-diffusion approximation. This approximation is limited by the assumptions of a collisional and weakly-ionized plasma. The low pressure within the thruster means that the plasma may not, generally, fall within the collisional regime. However, the presence of a magnetic field which induces azimuthal electron drift increases the mean free path of the electrons, implying that the plasma may be considered collisional at lower than normal pressures in a Hall thruster-like region [24]. Additionally, the electrons will undergo a spiral motion about the radial field lines, further increasing the amount of collisions within the discharge channel.

2.1.3 Source Terms

To model a plasma discharge, the production and loss of particles must be captured. Each inelastic reaction involves the creation and loss of particles, largely responsible for determining the density of the particles through the discharge. To calculate the reaction rates, experimental data is used to determine the probability of a certain collision. In this present case, this is in the form of collision cross-sections as a function of mean electron energy. Cross sections for specific reactions can be used to determine the reaction rate given a certain density and flux of the target and beam, respectively. The cross-section of a particular reaction, j, can be used to determine reaction rate as shown in Equation 2.17.

$$R_i = \sum_j \sigma_j x_j N n_e \nu_j \tag{2.17}$$

For certain reactions, the cross sections were used to determine a set of Townsend coefficients, as a function of electron energy. The Townsend coefficients are a measure of the number of collisions an electron will experience as it travels through 1 cm of the the plasma.

Below, Equation 2.18 shows the reaction rate as determined by the Townsend coefficients. The primary difference between using cross-sections and Townsend coefficients is that the reaction rate is based on the particle density with cross sections, while it is based on the total flux using Townsend coefficients. This provides a better description of the reaction rate when the ionization is driven by an electric field.

$$R_i = \sum_j \alpha_j x_j N |\Gamma_e| \tag{2.18}$$

2.2 Simulation of Electric Propulsion Systems: Literature Review

Simulations of EP devices are a vital component of the design process. EP devices are designed to operate in space, and so vacuum conditions must be created for effective testing. This requires large and expensive facilities, where testing time is in high demand. To optimize designs rapidly and cheaply, simulations are used. Recently, with the increasing popularity of EP devices, modelling has become more advanced and refined.

2.2.1 Ion Thruster Modelling

In 1988, Arakawa created an early computational model of an ion thruster [25]. This model uses a finite element method to solve a particle balance diffusion equation for the particle densities. Primary electrons are described by a velocity distribution function, neutrals by a constant density, and ions by ambipolar diffusion and ionization rates based on primary electron density. This simple model is able to generate useful results for cusped magnetic field structures. The "cusp" is a region where magnetic field lines converge, representing a region of high magnetic field strength. This model does not include conservation of energy, though insight into the plasma behaviour can be attained without its consideration.

More recently, in 2005, Wirz developed a hybrid 2-D computational discharge model to study plasma characteristics within an ion thruster, as well as scaling effects important for miniaturization [2]. The model included four species: primary electrons, secondary electrons, ions, and neutral particles. Primary electrons are treated using a particle-tracking method where each "particle" included in the calculations represents a collection of many actual particles. Motion and behaviour is then calculated based on the effects of the electromagnetic field. Secondary electrons are described by a Maxwellian velocity distribution with a depleted high-energy tail, at thermal equilibrium with the plasma. Ion densities are calculated based on ionization rates as determined by the electron densities. Ion fluxes are determined through ambipolar diffusion with corrections for non-classical diffusion across magnetic fields. Neutrals are treated as a "collisionless" gas, only colliding with walls and electrons. The effects of the grid on the thruster was included through an ion-optics code used to calculate a transparency for the grids. The effects of doubly charged ions are included by a correction factor based on the singly-charged ionization rate.

Wirz's work offers significant insight into ion thruster modelling, yielding results in close agreement with experiment. The discharge model created was then used to alter the thruster design, showing increases in overall thruster efficiency and consequentially in thruster lifetime. The primary increase in performance is achieved by strengthening the middle ring of magnets (Figure 2.1). This changes the discharge in such a way as to reduce the number of doubly charged ions present in the ion beam reducing waste power. Doubly charged ions will follow undesired trajectories, colliding with grids and creating a major source of loss and erosion in an ion thruster. This work illustrates how a computer model can inform and improve thruster design before testing.

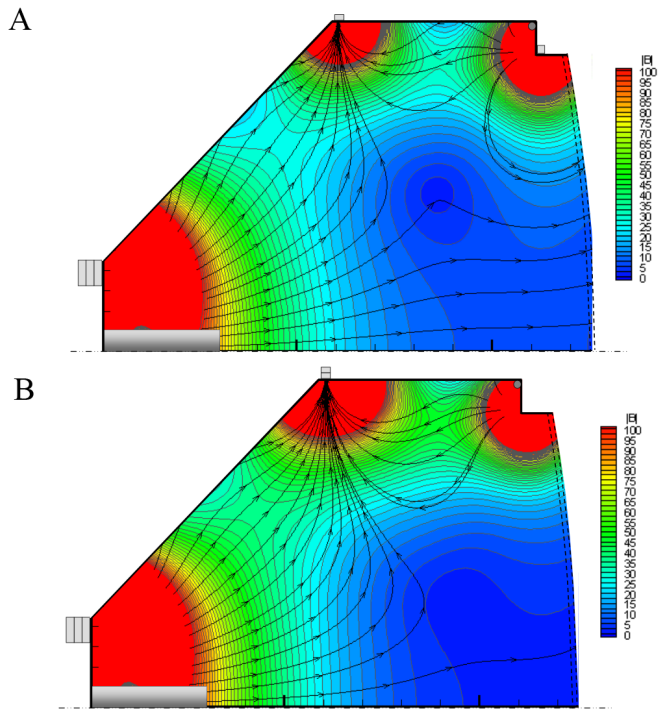

Figure 2.1: Magnetic field strength in the ion thruster modelled by Wirz. A) Unmodified magnetic field. B) Magnetic field with increased central ring magnet strength. [2]

2.2.2 Hall Thruster Modelling

Modelling a Hall thruster presents unique challenges compared to common plasma modelling. Primarily these are due to the cross electric and magnetic fields, and the importance of electron mobility across the magnetic field lines. Classically, electron mobility across field lines is described by Equation 2.19.

$$\mu_{e,\perp} = \frac{\mu}{1 + \Omega_e^2} \tag{2.19}$$

Here, Ω_e is the Hall parameter. This equation implies an inverse square relation between cross-field mobility and magnetic field strength. In experiments, this has been found to be inaccurate. This led to the proposal of an alternative to classical cross-field diffusion, termed Bohm diffusion. Equation 2.20 below shows the inverse relation, found to more accurately agree with experiments.

$$D_B = \frac{1}{16}\frac{k_B T_e}{eB} \tag{2.20}$$

However, Bohm diffusion, while an improvement over classical diffusion, still does not accurately describe a wide range of plasma discharges. For this reason, the unexpectedly high flow of electrons across magnetic fields is termed anomalous diffusion. Much of the difficulty in created a Hall thruster model is found in accurately reproducing anomalous, cross-field electron transport. Indeed, models generally rely on semi-empirical methods to correctly describe the cross-field electron transport, as the transport mechanisms are not precisely understood. Due to this, careful consideration must be given to treatment of electron transport across magnetic field lines.

2.3 Simulation Conditions

2.3.1 Modelling: Multiphysics Approach

In order to model the hybrid thruster, COMSOL Multiphysics software was used. This software package provides a set of physics modules which may be combined and customized to varying degrees. Using a commercial software package does require some prior verification of what can be accurately modelled. In the present case, the plasma modelling tools within COMSOL are based on the fluid equations, shown in Equations 2.5 to 2.7. These are further simplified using the drift diffusion approximation. While this method is applicable for a wide variety of plasma discharges, its accuracy does begin to degrade at very low pressures, when path lengths reach similar scale to the size of the discharge. This means that caution must be taken to ensure that the methods applied remain valid in the situations of interest.

However, developing a custom code to model the specific situation comes with its own drawbacks. In order to improve the accuracy of the model at low pressures, a particle or hybrid code would be required. The initial development of such a code is beyond the scope of this thesis, however, other disadvantages do occur with such a code. With a commercial code, design iteration is a quick and smooth process due to the in-built tools, and allows for multiphysics simulations. A custom code would require significantly longer to implement and test new geometries. Further, computational time is much lower using the a fluid-based model. The particle model operates by creating a number of "macro-particles", each of which represents a large number of actual particles. The motion of macro-particles is then simulated using standard equations of motion and electromagnetics. To attain accurate results with a particle-based

code, a minimum number of macro-particles must be used. Even using the minimum number of macro-particles required, simulations are often intensive. Long simulations further reduce the ease of design iteration. Additionally, a fluid code allows easy access to variables such as particles densities, fluxes, electric potential, and collision rates.

2.3.2 Model: Configuration and Key Parameters

Using the multiphysics approach described previously, a finite-element, time dependent 2-D simulation was implemented. Time dependence is a highly useful characteristic in the simulation as it allows for the evolution of the plasma to be observed. For example, the amplification of the plasma within the chamber may be seen, noting exactly how the fluxes of electrons interact with the applied electric fields. EP devices have the advantage of being able to easily turn on and off during operation. This is in contrast to chemical rockets, where restarting operation in space is more difficult. A time dependent simulation allows for the plasma ignition to be studied. It should be noted that the plasma ignition is an unstable discharge, and so accurate simulation can not be attained by a fluid code. However, knowledge of plasma behaviour and density can still be garnered.

An axisymmetric model was used as variables within the hybrid thruster are expected to be independent of the azimuthal direction. However, azimuthal variations do appear in Hall thrusters. These are azimuthal oscillations in the ion number density due to a variety of reasons, though a leading theory is the "predator-prey" oscillation between the neutral and electron densities [3]. Specifically, a build-up of electrons occur in the discharge channel due to reduced cross-field electron mobility. The build-up of electrons then causes a local increase in ionization, temporarily depleting the neutral density in this region. The reduced neutral density decreases the ionization until the neutral density is resupplied by the propellant feed. The cycle repeats, creating oscillations in the ion number density with azimuthal variation due to the azimuthal electron drift. Figure 2.2 shows time-lapse images of azimuthal plasma oscillations in a Hall thruster [3].

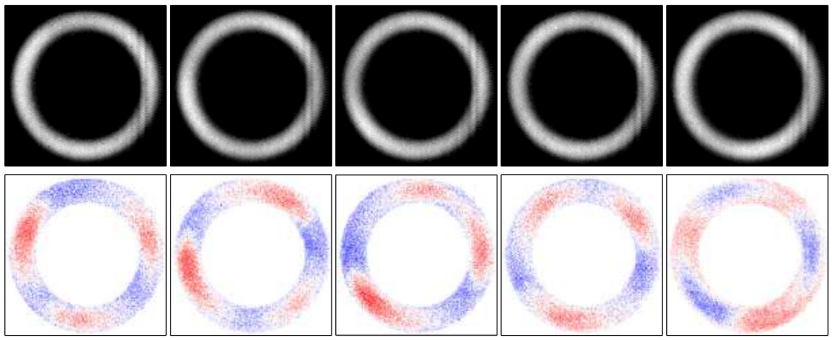

Figure 2.2: High speed video was used to capture time-lapse images of rotating spoke oscillations of ion number density. Contrast was enhanced using post processing techniques. Oscillations are visible as the brighter areas in the upper row, and the blue and red in the lower row. Brighter sections in the upper row (red in the lower row) represent regions of higher ion number density [3].

While the predator-prey oscillations are important to study (as they contribute to plasma instability and losses), the fluid code used here will not capture these oscillations. This means that a full 3-D simulation would not significantly increase the model accuracy.

2.4 Validation of Methods

Much like fluid dynamics, simulating plasma discharges presents a quandary. Simulation is used to study a particular scenario where experimental testing is infeasible. However, the question then becomes, how can the simulation be shown to be accurate, if there are no experimental results with which to compare? To answer this, the simulation method can be applied to a physical scenario for which experimental results are known and understood. In the present case, physically building and testing the hybrid thruster is infeasible. In place, a computer model was built, and would furthermore allow the investigation of small scale evolution The simulation method will be verified by comparing a simulated flat-plate, glow discharge with experimental results.

2.4.1 Glow Discharge

A glow discharge is maintained by creating an electric potential difference between two electrodes (high potential anode and a low potential cathode) with a low pressure gas (10 - 100 Pa) between them. Free electrons within the neutral gas are accelerated to the higher potential, ionizing neutral gas particles along their path, releasing more electrons. The ions are accelerated towards the low potential cathode, where they collide with the electrode, gaining an electron and knocking additional electrons off the electrode into the plasma. A glow discharge displays a few qualitative phenomena that should be reproduced in the simulations (Figure 2.3).

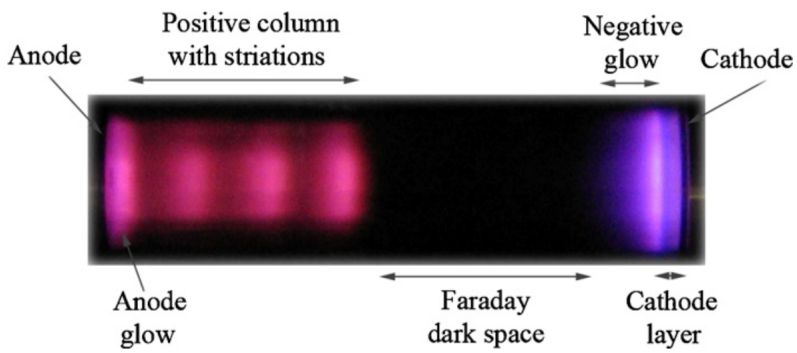

Figure 2.3: Photograph of the different regions present within a glow discharge, with major regions labelled. Figure from Livoskiy et al [4].

Regions within a glow discharge are named for the amount of light they produce, as this was the primary distinguishing feature of each section during the 19th century, when glow discharges were first being studied. The differing luminosity of each region reflect underlying physical phenomena occurring. Figure 2.3 shows a discharge with different glow regimes visible. Starting from the anode, the first region is the positive column. This represents a region of high electron current and low ion current. Due to the relatively low electric field, the electrons have enough energy to excite neutral atoms, but little ionization occurs in this region. The positive column is the region of the discharge responsible for the glow in neon signs. The Faraday dark space is the next region within the plasma, moving from cathode to anode. The electrons do not have sufficient energy to ionize neutral particles, and so the region appears dark. The next section, moving towards the cathode, is the negative glow. A high electric field in this region accelerates the electrons, causing an

avalanche of electrons and ions to be created. Within the negative glow, high concentrations of electrons and ions allow large amounts of recombination to occur. Recombination is largely responsible for the light from the negative glow. The electrons drift towards the anode and into the Faraday dark space, largely spent of energy due to ionizing collisions. The newly created ions drift towards the cathode, entering the cathode dark space. The cathode dark space is the area where ions are accelerated towards the cathode. Ions are able to gain sufficient kinetic energy to ionize neutral particles. The high kinetic energy of ions means that ionization collisions are more common than excitation, and hence the region is dark. In the final region, directly beside the cathode, is the cathode glow. Here, ions bombard the cathode, recombining with an electron from the surface and collapse to a ground state, emitting light.

In each of these different regions, the electric potential and currents of the various species are distinct. This allows for comparison between experimental results and the simulations. In experiments, emitted light is the most easily observed variable. However, the simulations do not account for the production of photons due to recombination and de-excitation. Looking at the electric potential, particle densities, and currents allows comparison with experimental results.

Figure 2.4 shows the electron density of a simulated Xe glow discharge at 50 Pa and a potential of 125 V. Near the cathode at the bottom, there is a very small region of low electron density. This is the cathode glow, and cathode dark space. Electrons are being released from the anode by ion collisions with the electrode, creating a slightly negative space charge. Electrons here are not energetic enough to ionize gas particles, so this very thin region appears dark. As the electrons are rapidly accelerated by the applied potential, they begin ionizing and exciting neutral particles, creating the cathode glow. The peak electron density is reached in the negative glow, which creates the brightest part of the discharge.

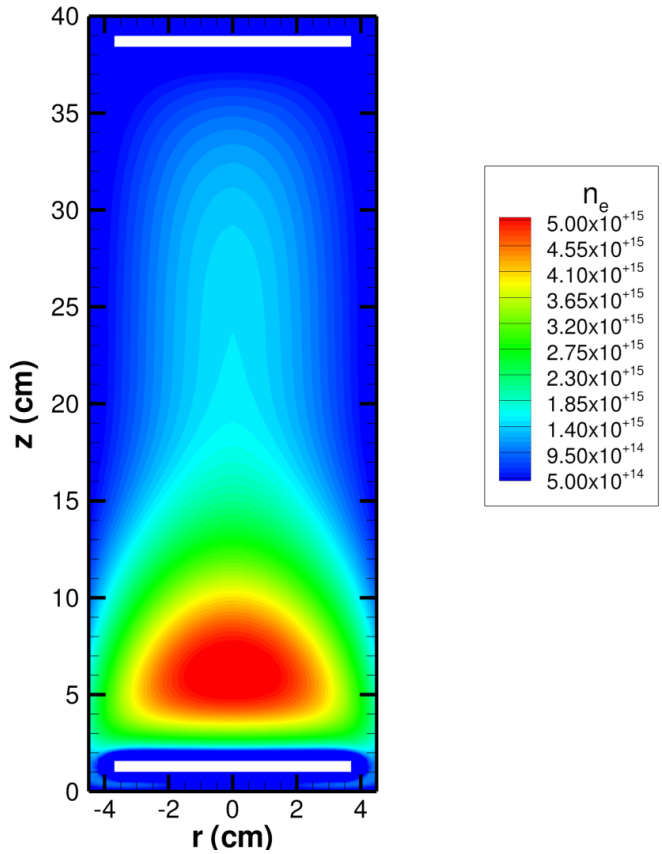

Figure 2.4: Electron density (m^{-3}) within the glow discharge simulation.

Subsequently, the electric potential begins to fall, creating the Faraday dark space and the positive column. This is a region of low electron energy and density. Finally, the electric field increases slightly near the anode (see Figure 2.5), creating the anodic glow region.

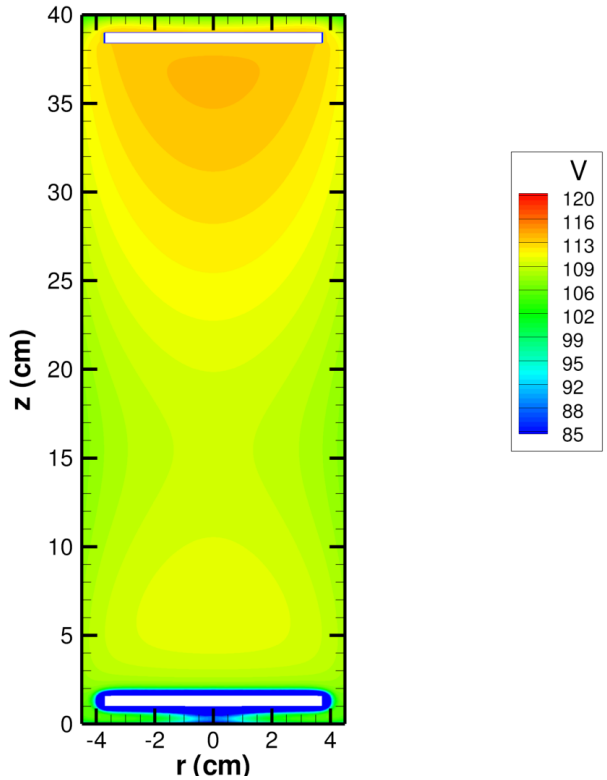

Figure 2.5: Electric potential within the glow discharge simulation.

Peak electron number densities are also within expected values for a glow discharge. Shown in Figure 2.6, experimental results from Lisovskiy et al give a peak electron number density for a glow discharge at 80 Pa with an applied electric field of 10000 V/m as approximately 1.4×10^{16} m^{-3} [26]. The glow discharge model here operates at a lower pressure with a far lower electric field, leading to a lower but comparable peak electron number density of 1.4×10^{16} m^{-3}. The modelling method used here generates phenomena and comparable results to those of experiment, and so will be considered of sufficient accuracy for the proposed task.

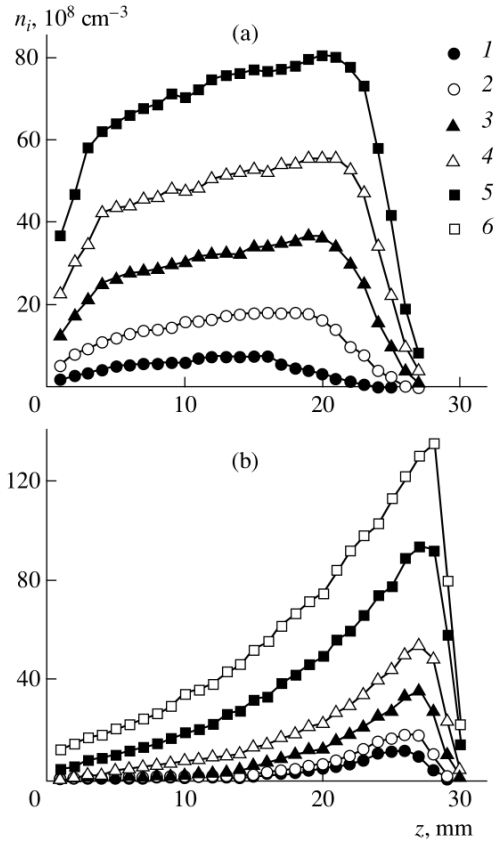

Figure 2.6: Electron number density in a glow discharge at a) 13 Pa, where the applied potential is 1) 350 V, 2) 400 V, 3) 500 V, 4) 600 V, and 5) 700 and b) 0.6 torr, where the applied potential is 1) 300 V, 2) 325 V, 3) 350 V, 4)375 V, 5) 400 V, and 6) 425 V [4].

2.4.2 Mesh Sensitivity Analysis

To ensure that the simulation was not affected by the mesh size, a mesh sensitivity analysis was undertaken. This was conducted using the glow discharge experiment previously studied for validation purposes. The same simulation was run for three different mesh sizes, then results analyzed to determine if the mesh had an effect.

Figure 2.7 shows the simulation run for three different mesh sizes. Results for each mesh size were nearly identical, indicating that the results were unaffected by mesh size for the purposes of this work. Figure 2.8 shows the

electron density along the centre line of the glow discharge all mesh sizes. It is clear that the mesh had no noticeable effect on the simulation results.

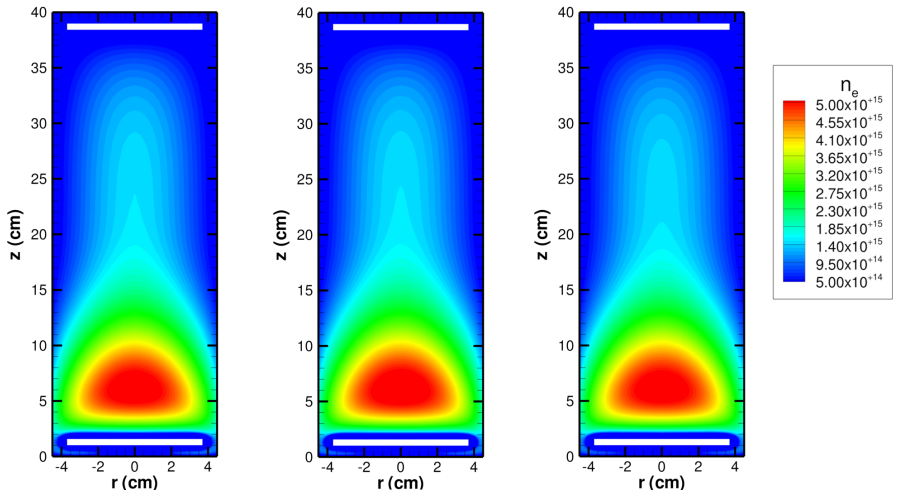

Figure 2.7: Electron density within the simulation using a mesh of (from left to right) 9000, 16000, and 32000 cells.

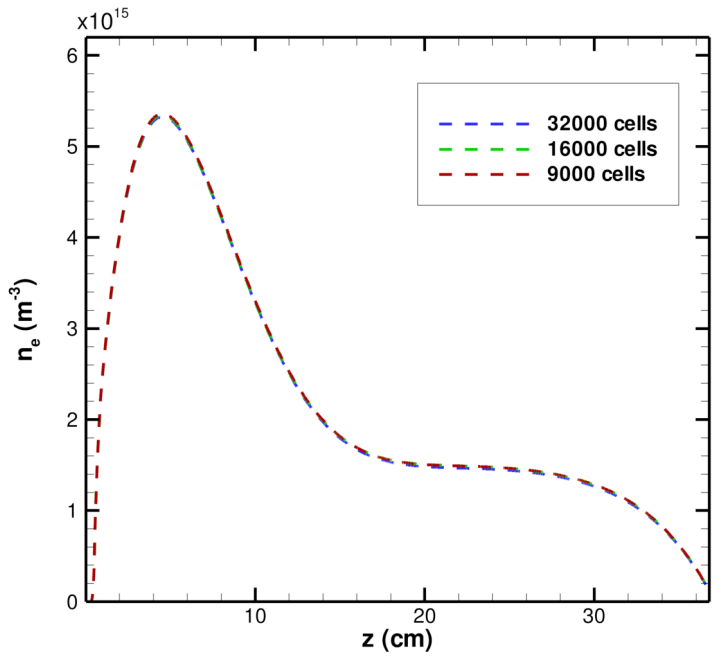

Figure 2.8: Comparison of electron density of the glow discharge along the axis for each mesh size.

2.5 Concluding Remarks

Plasma is a state of matter which behaves differently than other conventional forms, such as fluids or gases. The presence of free charged particle means that electric and magnetic effects are important on the macroscopic scale. Application of a variety of different methods to different electric propulsion types have been discussed. The formalisms used to model the hybrid thruster have been discussed and their applicability has been tested. The following chapters will focus on the unique issues faced in creating a hybrid Hall-ion thruster, as well as discussions of the results of the simulations.

3 Hybrid Electric Spacecraft Propulsion: Conceptual Design

3.1 Hybridization Considerations

In designing a Hall/ion hybrid thruster, there are a variety of factors that determine the improvement and success of the device. One of the most obvious and perhaps largest source of mismatch between the two thrusters types is the plasma regime they operate under. A Hall thruster operates at a higher neutral pressure with a stronger magnetic field. An ion thruster operates at a lower pressure with a much weaker magnetic field. Consideration must be given to how these different plasma conditions will interact and transition from one to the other. Ion thrusters generally operate with neutral densities of approximately 10^{18} m^{-3} to 5×10^{18} m^{-3} within the plasma discharge while Hall thrusters often operate at a range between 10^{18} m^{-3} and 10^{20} m^{-3}. The higher density within a Hall thruster is generally only in the region of the propellant feed. The short and open nature of the Hall thruster discharge channel means that the ion number density varies considerably over the length of the channel. The majority of the discharge takes place in a region where the neutral density is around 10^{18} m^{-3}.

Creating a low neutral density inside the ionization section and a higher neutral density inside the Hall section is infeasible, as pressure differences will quickly equalize any density difference created, especially as the Hall section is able to allow neutral particles to escape entirely while the ion section contains them. Instead, the total neutral density in the ionization section was increased to a level closer to that of the Hall thruster, though not far greater than what is found in any ion thruster. This has two primary effects. First, the same ionization rate as within a standard ion thruster can be maintained with a lower

electric field. Second, in regards to simulation accuracy, the higher pressure ensures the assumptions required for the drift-diffusion approximation remain valid.

3.1.1 Hybridizing the Magnetic Field

Another important difference between Hall and ion thrusters which must be considered is the magnetic field. With an ion thruster, a set of ring magnets establish high magnetic fields near the discharge chamber walls (see Figure 1.4). The fields are largely parallel to the chamber walls, preventing electrons from quickly reaching the walls and being lost. In the majority of the discharge, the magnetic field is low and does not have a large effect. A Hall thruster uses a strong magnetic field to inhibit the electrons' axial motion. This confines the electrons to a small segment of the discharge channel, where they travel around the radial magnetic field lines, ionizing the neutral propellant.

In merging a Hall and ion thruster, attention must be paid to keep the primary magnetic field functioning in one section without interfering with the other. To accomplish this, a ring cusp structure was tested within the ionization section in such a way as to reduce the magnetic field near the transition region (see Figure 3.1). Any radial magnetic field components near the transition region hinder the electron's ability to enter the acceleration section. Electrons must be able to enter the acceleration section in order to maintain quasi-neutrality. The ring-cusp structure is also shaped in such a way as to prevent losses to the inner "hub" (Figure 3.2), by placing magnets on the hub to create a higher magnetic field along its walls. Within the acceleration channel, two rings of magnets were used to create a magnetic field topology similar to that of a Hall thruster. One difference is that the magnetic circuit is completed by flux channels which go around the outside of the simulation domain (above the exit boundary in Figure 3.1). This was done to create a complete magnetic circuit, preventing the magnetic field lines from intersecting the plasma a second time. In an actual Hall thruster, the magnetic flux is carried around the anode at the bottom of the discharge channel. A central coil and a set of axially aligned coils around the perimeter of the thruster direct the magnetic flux such that it does not cross the plasma a second time (as all magnetic field lines must form complete loops). In the hybrid thruster, the magnetic flux will be carried through the three supports that hold the central hub in place. However, the axisymmetric nature of the simulation prevents the inclusion of these subs in the model here. Further investigation into the effects these supports would have on the discharge performance are warranted.

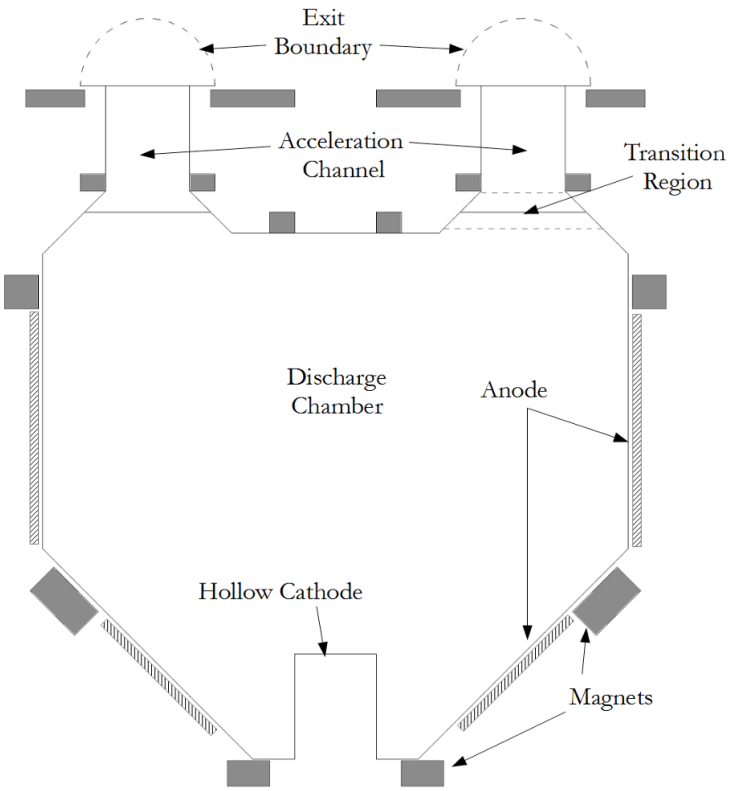

Figure 3.1: Schematic of the hybrid thruster design tested, with key components and regions labelled. Dark grey regions represent magnets, hatched regions represent the anodes.

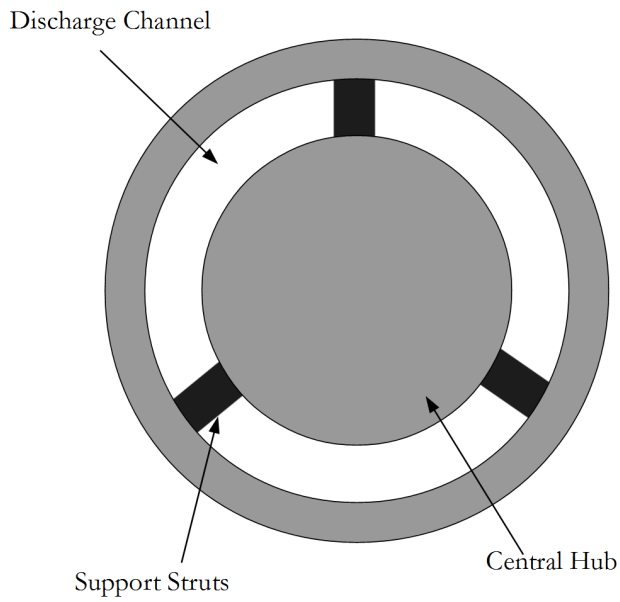

Figure 3.2: Front view of a potential support strut configuration for the hybrid thruster.

3.1.2 Hybridization of Electric Fields

An additional difference introduced by the hybridization of the thruster is the removal of the anode from the Hall thruster section. Generally, a Hall thruster will have an anode at the bottom of the discharge channel which, in conjunction with the cathode, establishes the axial electric field. In the hybrid thruster, the anode is replaced by plasma at the discharge potential. Ideally this will establish a similar radial electric field to that found in a Hall thruster, though the lack of a physical electrode may shift the electric field. This is important as the Hall section relies on the $\overrightarrow{E} \times \overrightarrow{B}$ term to create its azimuthal electron current.

Both Hall and ion thrusters must neutralize the ejected ion beam. This is done to prevent charge build-up on the spacecraft as well as to prevent beam stalling. Beam stalling occurs due to the buildup of positive charge outside the thruster. The purely positive beam will increse in electric potential until it is equal to the accelerating potential within the thruster, at which point ions will no longer flow. The most common method of neutralizing the ion beam is by using an neutralizing hollow cathode. A neutralizing cathode also serves

an additional function. Some of the electrons ejected by the cathode enter the Hall section and aid in maintaining the discharge and quasi-neutrality within it. Lastly, the neutralizing cathode helps to establish the axial electric field responsible for creating thrust.

Hall and ion thrusters generally operate at separate discharge potentials. A conventional ion thruster often operates at an acceleration voltage of 1100 V, allowing for high I_{sp} [13]. Compared to this, Hall thrusters usually have an acceleration voltage of 300 V to 500 V. The primary reason for this is that Hall thrusters begin to experience large plasma instabilities at discharge potentials above approximately 500 V. The plasma instabilities produce prohibitively high losses in efficiency due to their creation of large numbers of doubly charged ions. One of the potential advantages of a Hall/ion hybrid thruster is the ability to maintain a stable discharge at higher voltages while using a Hall-like ion acceleration. The simulations here explore a variety of different acceleration potentials.

3.2 Hybrid Thruster Concepts: Modelling

Previous attempts to create a hybrid thruster have been discussed in literature. For example, in 2004, Peterson created and tested a hybrid thruster device [5]. The device had an ion thruster style discharge chamber, with a Hall thruster style acceleration stage coupled to the exhaust (see Figure 3.3). The rationale behind this configuration is that it may allow a Hall thruster to attain a higher I_{sp}. Generally, Hall thrusters are not operated at discharge potentials as high as ion thrusters as plasma instabilities begin to occur, causing large losses. It was hoped that by adding an ion thruster discharge chamber that the higher potential used would not create plasma instabilities. The thruster achieved stable operation, however it was not able to achieve the efficiency desired. In particular it was thought that a large amount of electrons were leaking across the magnetic field in the Hall-stage of the thruster. This lowered the useful acceleration potential and reduced the effectiveness of the thruster. This large electron leakage was suspected to be due to the four magnetic flux shunts. These are supports which held the central hub in place in the centre of the Hall-stage. The shunts also carried the magnetic flux in order to create the required magnetic circuit for the Hall thruster segment. During operation, it was observed that the Hall current of electrons was colliding with flux shunts, thereby reducing their energy and allowing them to leak across the magnetic field. Additionally, the discharge potential was limited to 600 V due to contamination of the magnetic circuit materials. With the removal

of the flux shunts and better material used for the magnetic circuit, Peterson expects the thruster to operate effectively at over 1000 V.

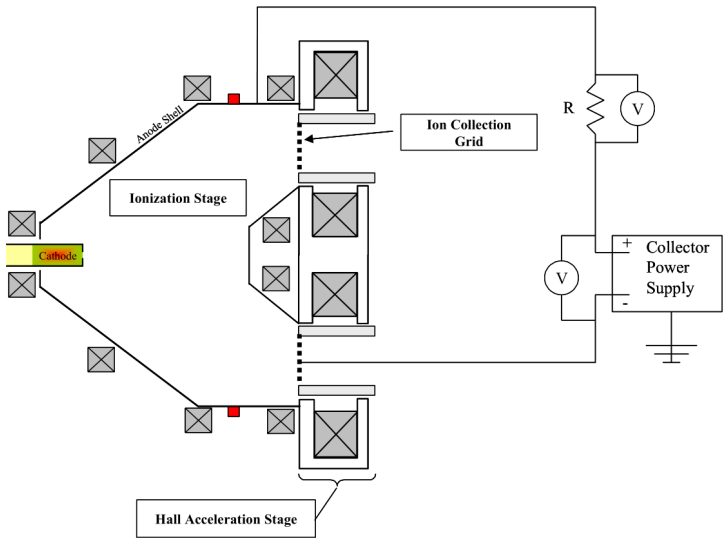

Figure 3.3: Cross sectional schematic of the NASA-173GT [5].

Other work in a novel Hall thruster geometry was conducted by Yu et al [6]. This work involved the creation of a two-stage Hall thruster (see Figure 3.4). An ionization stage was created in which annular magnetic field confinement is established, preventing electrons from reaching the chamber walls. An intermediate electrode was introduced that serves as the cathode for the ionization stage and the anode for the acceleration stage. The acceleration stage is similar to a conventional Hall thruster design. The magnetic field is shaped in such a way as to create a zero magnetic field region between the ionization and acceleration stages.

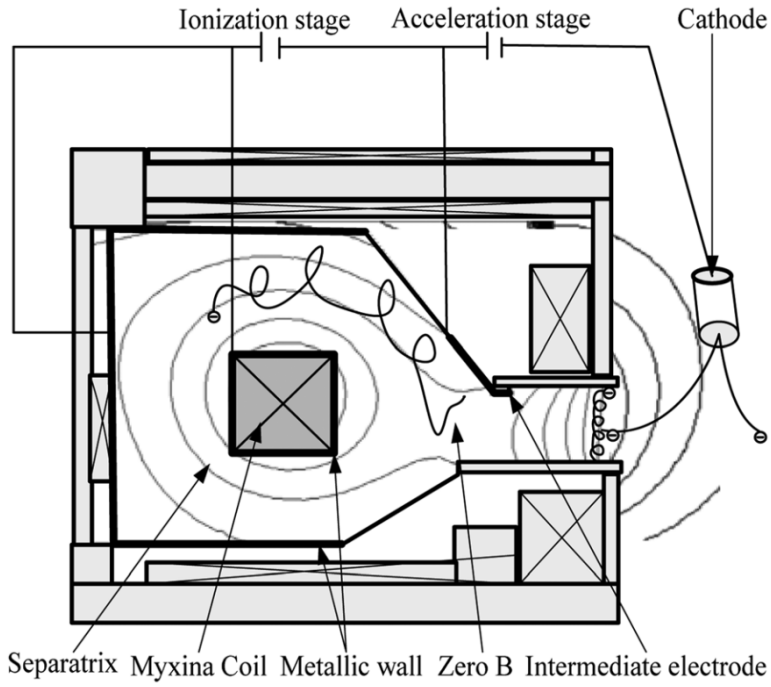

Figure 3.4: Cross-section of the double-stage Hall thruster, with various components labelled [6].

Hall thrusters have been shown to perform well for station-keeping missions [27]. However, they are not as ideally suited to orbit transfer missions that may require greater thrust and discharge potentials. In order to meet this demand, Yu proposes that the ionization and acceleration of the ions be largely separated, allowing an overall greater number of ions to be created while accelerating them to higher velocities. This work concluded that it is difficult to independently control the ionization and acceleration. This is due to the fact that ionization will occur in both areas.

Another thruster concept that differs from the more standard Hall and ion thruster is the High Efficiency Multistage Plasma (HEMP) thruster [28]. The HEMP thruster uses a series of alternating polarity magnetic rings to create magnetic cusps (shown in Figure 3.5). An axial electric field is created by an anode at the back of the discharge tube and the neutralizing cathode outside the thruster. The magnetic cusps impede the axial motion of the electrons, trapping them within the plasma. Circling about magnetic field lines, the trapped electrons then ionize the neutral gas particles. The axial electric field

then accelerates ions out the back of the thruster.

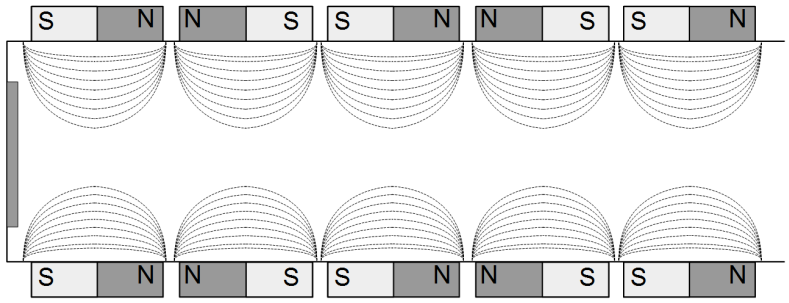

Figure 3.5: Schematic of the magnetic geometry with the HEMP thruster.

Recently, simulation work was conducted on a micro-HEMP thruster to try and gain a better understanding of the scaling effects [29]. Multiple modelling methods were used to study different areas of interest. To study the general plasma behaviour, a fluid-based simulation was carried out on both the electrons and ions. This simulation was run for 10 ns, but still produced valuable information about the plasma densities. A particle model was used to better understand the effects of magnetic mirroring on the plasma. Magnetic mirroring is an effect that occurs as a particle travels through an area with an increasing magnetic field (converging magnetic field lines). The particle's velocity perpendicular to the field lines will increase due to the Lorentz force. However, assuming no other forces are acting on the particle, the kinetic energy of the particle must remain constant, and so the velocity parallel to the magnetic field lines will decrease. This mirror effect is very important to the electron confinement within a HEMP thruster. However, this effect is often neglected in fluid-based, simulation software.

By combining elements and ideas from previous thrusters, a hybrid thruster will be designed, attempting to capture the beneficial aspects of each thruster component. The evolution of the species governing the plasma and the fundamental parameters will be discussed.

3.3 Hybrid Thruster Design: Components

3.3.1 Design Overview

The hybrid thruster model created in this work consists of a ring-cusp ion thruster ionization chamber coupled to a Hall effect thruster acceleration section. A schematic of the thruster is shown in Figure 3.1, and each subcomponent will be discussed hereafter.

3.3.2 Discharge Chamber

The purpose of the discharge chamber in the hybrid thruster is to ionize the neutral gas particles. As with a ring-cusp ion thruster, electrons are emitted by a hollow cathode into the discharge chamber. An electric field established between the cathode and anode accelerate the electrons until they have enough energy to ionize gas particles upon collision.

The design of the discharge chamber is similar to those found in ring-cusp ion thrusters, with modifications made to adapt for the annular acceleration stage. A conical shape is used instead of a cylindrical shape to reduce electron losses to the walls. Cones have a smaller surface to volume ratio than cylinders, so using a cone shape where possible reduces potential surface losses while maintaining volume for the discharge. A spherical chamber would minimize electron losses, but complicates fabrication. The annular acceleration stage was included by removing the grids from a ring-cusp ion thruster and replacing them with a central "hub". The hub contains the magnets required to establish a Hall thruster style magnetic field in the acceleration stage. While not included in this simulation, the central hub requires support struts to hold it in place. The supporting struts would allow for the magnetic circuit of the acceleration section to be closed without crossing the discharge. The magnetic flux that crosses the acceleration channel in one direction must return to the original magnets, as all magnetic field lines must form closed loops. Magnetically conductive materials are required to guide the magnetic flux, without it returning across the plasma. Figure 3.2 shows a proposed configuration of the support struts.

The lowest number of struts required should be used, so as to reduce the amount of surface area exposed to the discharge. Additional surface area will increase the losses in the plasma by absorbing electrons and neutralizing ions. Additionally, total weight should be minimized where possible, for all devices being lifted to space. Each strut carries magnetic flux between the two rings of magnets on either side of the acceleration channel. The magnetic flux is

more easily carried with more flux struts, as this will minimize the path length of the magnetic circuit. The design proposed here makes use of three sturts, though 3D simulations will be required to determine the minimum number of acceptable struts.

3.3.3 Hollow Cathode: Electron Source

A vital element of any ion of Hall thruster is the cathode acting as an electron source. In an ion thruster, two cathodes are required. The first cathode creates electrons that are ejected into the discharge to maintain and create the plasma. A second cathode is required outside the main thruster to neutralize the ejected ion beam, preventing the build-up of charge and preventing beam stalling. In a Hall thruster, a neutralizing cathode is also required outside the main discharge, for the same reasons. Additionally, in a Hall thruster, the neutralizing cathode provides electrons that seed and ignite the discharge.

Cathode is a general term for an electrode that emits electrons (or, into which positive charge flows). In EP, cathodes generally take the specific form of a hollow cathode. A hollow cathode is able to reliably produce high currents of electrons without breaking down quickly due to erosion. Cathodes tend to be prone to degradation caused by high temperatures, where materials soften and particles bombard them at higher energies. Figure 3.6 shows a diagram of a hollow cathode, with the main components.

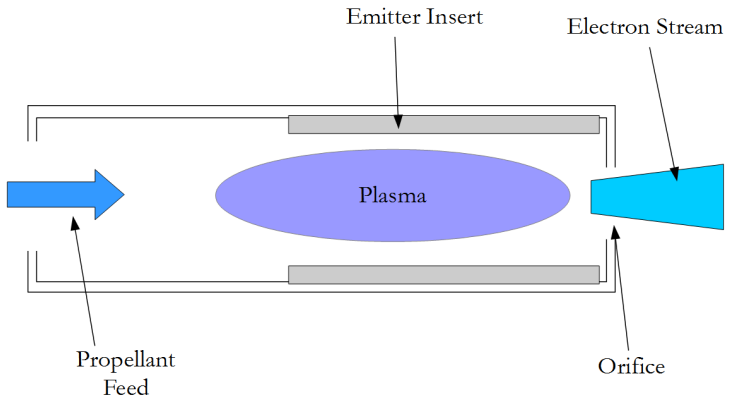

Figure 3.6: Schematic of a hollow cathode assembly, showing various components.

A hollow cathode consists of a metal tube with an emitter material along

the inside of the walls. There is a small hole called the orifice at one end, with the other end being fed by a stream of gas. A heater around the outside of the metal tube is used to heat the assembly to the point where the emitter material will emit electrons due to thermionic emissions. The emitted electrons ionize the gas particles, releasing secondary electrons in the process. The secondary electrons and newly created ions will collide with the walls and the emitter material, depositing energy and heating the material. Additionally, as ions and electrons are forced out through the narrow orifice, the local resistance increases. The increased resistance creates a region of high temperature, heating the walls of the hollow cathode. Eventually the heating coil around the hollow cathode can be turned off, and the device will function in a self-heating mode.

3.3.4 Acceleration Channel

The acceleration channel of the hybrid thruster is where many of the potential benefits as well as issues may occur. In an ion thruster, the acceleration system is a set of grid electrodes. The grid electrodes extract and acceleration positive ions, which confines the electrons in the discharge chamber. In a Hall thruster, the acceleration occurs in a quasi-neutral environment. The difference between the two systems is that the Hall thruster total beam current is not limited by space-charge. Due to the purely positive beam of the ion thruster, the beam current eventually saturates, limiting the total thrust that can be created at a given power level. However, an ion thruster is able to create higher exhaust velocities compared to a Hall thruster due to its higher acceleration potential. At higher potentials, Hall thrusters begin to undergo large discharge instabilities which greatly reduce efficiency and lifetime.

The acceleration channel in a Hall thruster is also the life limiting component. High ion and electrons temperatures lead to high sputtering rates, wearing down the dielectric surfaces on the inside of the channel. Recently, Conversano et al. successfully designed a magnetically shielded Hall thruster [7]. By varying the shape of the magnetic field within the discharge channel such that the magnetic field lines did not impinge directly onto the surface of the outer channel wall (as shown in Figure 3.7), the erosion rates on the outer walls were reduced by three orders of magnitude.

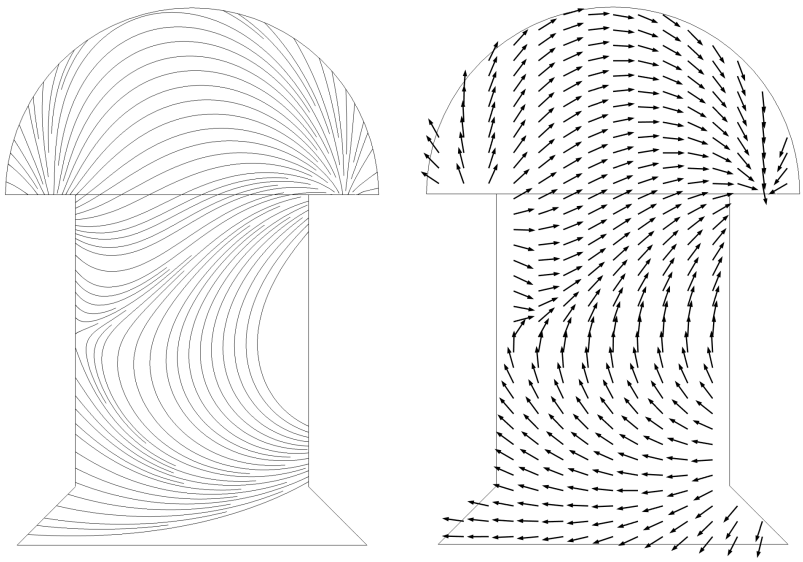

Figure 3.7: Acceleration channel of a Hall thruster with magnetic field lines shown, demonstrating the magnetic shielding technique of Conversano et al. [7]

Additionally, the acceleration channel is responsible for the formation of the ion beam. The magnetic field shape within the channel will affect the shape of the electric field, as the electrons will tend to equalize the potential along field lines. By shaping the magnetic field, the beam divergence angle can be influenced. Large beam divergence angles can be a major source of officiency loss in a Hall thruster. This kinetic energy has been imparted to the ions, however, the momentum is not being transferred to the spacecraft. To try and reduce the beam divergence, a variety of different magnetic field shapes will be tested.

3.3.5 Magnetic Field

The magnetic field within the ionization stage is modelled after a ring-cusp ion thruster. The field is weak within the majority of the ionization stage, but increases in strength near the thruster walls. This configuration is used to reduce the flow of electron to the walls, lowering electron losses. Additionally, a strong magnetic cusp region was created in the acceleration stage to contain electrons within the chamber. Figure 3.8 shows the general distribution of the magnetic field.

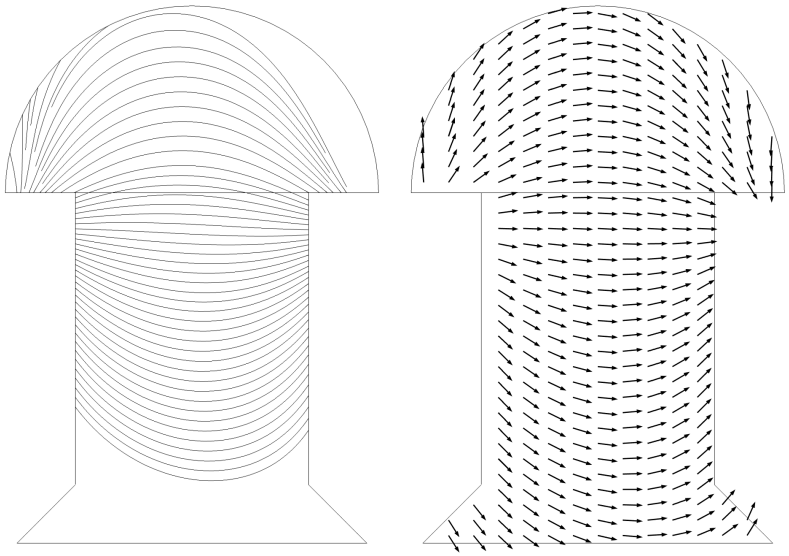

Figure 3.8: Magnetic field lines within the hybrid thruster.

The magnetic field within the ion thruster portion of the hybrid thruster is based on the ring cusp with some modifications made to account for the addition of the central "hub". A magnet was added to the hub to produce a magnetic field which would reduce electron losses to the central walls.

The magnetic field is of crucial importance with an ion or Hall thruster. In an ion thruster, the magnetic field greatly enhances the ionization rate within the discharge chamber. This is achieved by using what is termed a ring-cusp structure for the magnetic field geometry. An example of this magnetic field geometry was shown in Figure 1.4. By creating a strong magnetic field which is roughly parallel to the thruster walls, ions are held inside the discharge chamber. Electron mobility is greatly reduced across magnetic field lines. By confining the electrons to remain in the discharge, the probability of an ionizing collision is increased, leading to overall greater discharge efficiency.

Perhaps even more so than in an ion thruster, the magnetic field within a Hall thruster is vital to its function. A strong radial magnetic field is created through the Hall discharge channel, as shown in Figure 3.9. This field serves a dual purpose. First, the radial magnetic field greatly reduces the axial mobility of the electrons. This prevents the electrons from flowing directly from the cathode or discharge directly to the anode. By impeding their axial motions, the electrons are trapped in the ionization region for a longer period

of time, enhancing their ionizing collision probability. Additionally, because there is an axial electric field in the region of the radial magnetic field, an azimuthal drift of electrons is created due to the Hall effect. Further, the radial magnetic field lines cause the electrons to travel in a cyclical motion. Ensuring the the electrons are able to cycle freely within the discharge channel is a central consideration in designing a Hall thruster discharge channel

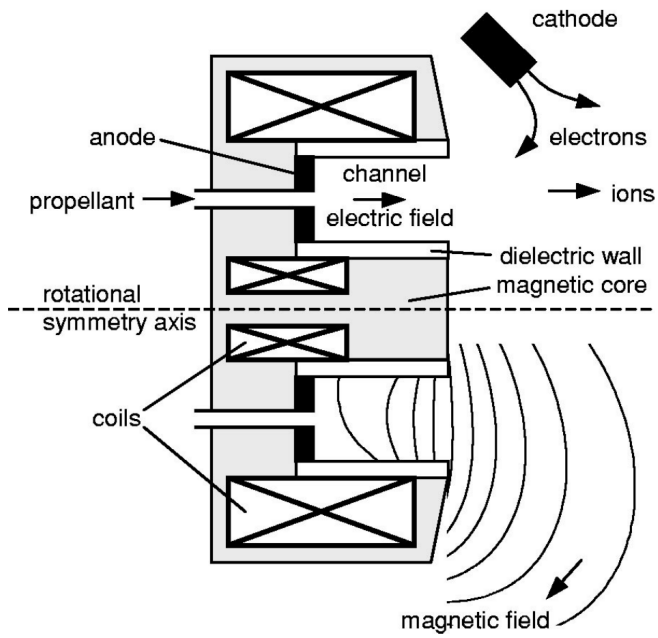

Figure 3.9: Schematic of a Hall thruster, with magnetic field lines also shown [8].

An important note concerning the magnetic field is that due to the hybrid nature of the thruster, the magnetic field of a Hall or ion thruster could not be directly replicated pas part of the simulations here. Specifically, a Hall thruster uses a magnetic circuit to redirect the magnetic flux around the discharge channel. This ensures the magnetic field within the discharge is purely one direction, and removes and cusp structure that may occur. Due to the axisymmetric nature of the simulations conducted here, the magnetic field flux had to be redirected around the plasma channel by creating a magnetic circuit which extended above the discharge. This is not realistic of course, but serves to produce the desired field. In the actual thruster, the magnetic

circuit will be directed through the central portion supports. However, the 2D nature of the simulations means the effect of the supports on the plasma could not be filly explored. Future work could be undertaken to create a full 3D model of the thruster, and explore the losses related to the addition of these supports.

3.4 Hybrid Thruster Model Specifics

To model the thruster, an axisymmetric, time-dependent simulation was conducted. This allows for shorter simulation times, as well as the ability to observe the evolution of the plasma towards steady-state. This would correspond, in principle, to the start-up of the thruster in practice, with a steady-state trend emerging if the simulations are run for a longer period.

The discharge is maintained by a 35 V potential difference between the cathode and the anode (see Figure 3.1). The electric potentials were ramped-up over 100 ns to more accurately model the rise time of real electrodes, while also aiding in the stability of the simulations. A finite rise time reduces the appearance of arcing, which the simulation equations will not be able to handle. The external boundary condition is set at ground potential to simulate the effects of the neutralizing hollow cathode.

The xenon discharge model being used contains singly charged ions, electrons, background gas, and an excited xenon species, found to be the most dominant at the electron energies of interest. Specifically, Equations 3.1- 3.4 give the reactions which are included in the plasma model. While a great many excited xenon species may occur, they are often at similar excitation energies. The species selected here has a much greater cross section than other excited species at the energy of interest, and so other species were neglected.

$$Xe + e^- \rightarrow Xe + e^- \text{ Elastic} \tag{3.1}$$

$$Xe + e^- \rightarrow Xe^+ + 2e^- \text{ Ionization} \tag{3.2}$$

$$Xe + e^- \rightarrow Xe^* + e^- \text{ Excitation} \tag{3.3}$$

$$Xe^* + e^- \rightarrow Xe^+ + 2e^- \text{ Stepwise Ionization} \tag{3.4}$$

Collision cross sections were taken from LXCAT databases [30]. The cross sections are given as function of electron energy. From this, a two-term approximation of the Boltzmann equation is solved to generate swarm coefficients for

the ionization reactions [31]. The plasma coefficients were used to generate reaction rates for the ionization reactions as they provide a more accurate description of the ionization inside a direct current discharge. Direct ionization of neutral background gas, as well as the two-step ionization of an excited atom are considered. In addition, elastic collisions of electrons with Xe atoms are included.

Due to the electric and chemical nature of plasma, the surface interactions which occur must be taken in account. In the thruster simulations carried out here, two interactions are of interest. All ions are immediately lost on contact with thruster walls. It is assumed that they are able to recombine with an available electron without hindrance. Additionally, all excited species which contact the thruster walls undergo de-excitation, reverting to neutral, ground-state atoms. Wall heating effects are not included in these simulations. Electrons which contact the walls are also assumed to be lost. In the case of the metal electrodes, the electrons will not build up on the surface due to the applied potential.

To maintain the discharge, the effects of a hollow cathode are also included in the model by the addition of a flux of electrons. The flux of electrons is added as flowing out of a an orifice, as shown below in Figure 3.6. This flux and the applied potentials formed the source of ionization within the thruster. Additionally, a small stream of ions is generated by the hollow cathode due to the propellant being passed through and electrons being generated within it.

The cathode and anode are modelled as metallic electrodes. All other solid surfaces are modelled as dielectrics with a dielectric constant of 7. This is done to model the boron nitride commonly used in constructing Hall thrusters. The dielectric surfaces were modelled using Equation 3.5. Integration of a Hall and ion thruster requires consideration of magnetic and electric field profiles. The different plasma regimes, ionization, and ion acceleration must be accounted for in order to produce an efficient, functioning thruster.

$$\frac{\partial \rho_s}{\partial t} = \overrightarrow{J_e} + \overrightarrow{J_i} \tag{3.5}$$

The exit boundary of the hybrid thruster simulation is meant to represent the plasma plume and outer space. For this reason, all electrons or ions which contact the outer boundary region are considered lost. The plasma in the plume of a Hall thruster rapidly drops to zero potential due to the neutralizing cathode injecting electrons into the ion beam. To model this rapidly dropping potential, the external boundary is set to 0 V. Curving the exit boundary was done in order to match the shape of the magnetic field in that region. Electrons tend to flow along magnetic field lines, and so electric potential

equalizes along the field lines. The curve of the exit boundary matches the shape of the magnetic field lines, and consequently the equipotential lines as well.

3.5 Concluding Remarks

Combining an ion and Hall thruster to create a hybrid thruster with improved performance provides a set of unique challenges. Consideration must be given to the different plasma regimes in each device, as well as the different components that must be efficiently coupled. Each component of the plasma evolution within the hybrid thruster has been discussed in detail. Simulation results of the hybrid thruster design will be discussed further in the Chapter 4.

4 Simulation and Hybrid Thruster Results

4.1 Introduction

The hybrid thruster design outlined in the previous section is modelled and results are discussed in this section. The time evolution of the species within the plasma for the hybrid design configuration (shown in Figure 4.1) is explored hereafter. Plasma characteristics are governed by the interaction of electron, ions, and neutral gas particles. The dynamics of each of these plasma components predominantly occur at different time scales. Electrons will respond to electromagnetic fields on the scale of nanoseconds due to their low mass. Ions also respond to electromagnetic forces, however, they weigh thousands of times more than electrons, and so typically respond on the scale of microseconds. Neutral gas particles are driven by diffusion and pressure gradients, generally occurring on the scale of milliseconds. For this reason, the results of the time dependent simulations will be studied at a variety of time-scales. Furthermore, there are plasma subregions within the thruster where different behaviours are observed. Additionally, the effects of different model parameters on the performance of the thruster will be tested. Parameterizations will be conducted on the hybrid thruster in an effort to improve performance. Results of the simulations and the plasma evolution will be compared to those of existing Hall thrusters.

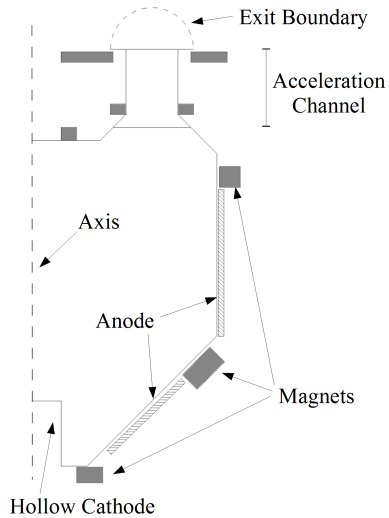

Figure 4.1: Axisymmetric cross section of the hybrid thruster (see also Figure 3.1). Grey regions represent magnets.

4.2 Time Evolution

4.2.1 Initiation of the Discharge

Early results will focus on the first structures formed in the simulation domain, after 10 ns have elapsed. The initial conditions play a large role in the early simulation results, as much of the simulation has not yet responded to the source terms, however, they do not affect the steady-state results. Additionally, many variables in the simulation are introduced gradually over 100 ns using a ramp function. This is done for two reasons. First, gradually turning on source terms will more accurately match the time profile of the source terms in reality. For example, the electrodes and hollow cathodes will have a non-zero rise time. Second, gradually introducing source terms allows for more stable simulations compared to starting the simulation with source terms at full value. It should be noted that the ramping of electric potentials is also present in experiments.

At 10 ns, the main structure which is apparent in the results is an increase in the ion number density downstream of the interior hollow cathode (Figure 4.2). Electrons provided by the hollow cathode are injected directly and accelerated towards the electrodes on the discharge chamber walls. How-

ever, the short time frame has not yet permitted the electrons to move any significant distance towards the electrodes.

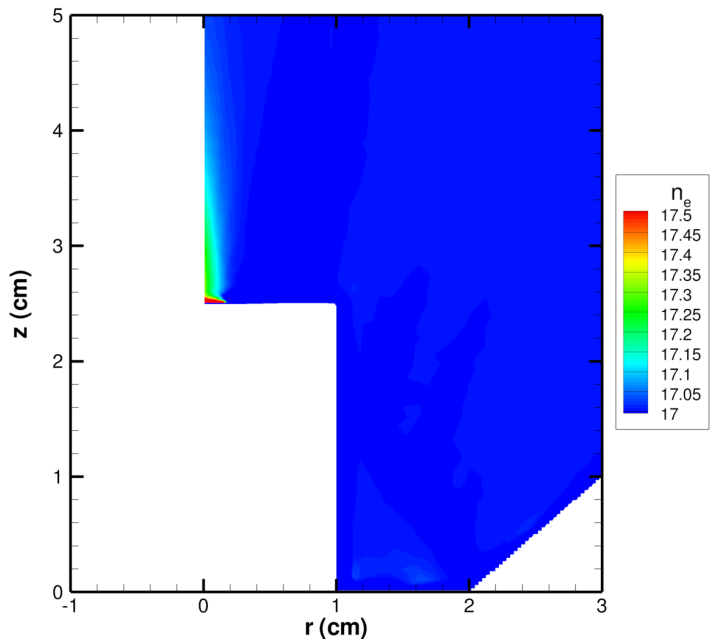

Figure 4.2: Log of electron number density (m^{-3}) after 10 ns showing the effect of the hollow cathode.

Additionally, the ground potential along the exit boundary has repelled the electrons, as seen in Figure 4.3. At this early stage in the discharge, the plasma is in the process of being created. In an actual thruster, electrons and ions would be leaving the hollow cathode and being injected into the centre of the discharge chamber. Aside from the narrow jet of plasma, the remainder of the discharge chamber would be filled with neutral gas. In the simulations conducted here, the initial conditions create slightly different conditions. A low but uniform density of 10^{14} m^{-3} electrons and ions is in place in the simulations.

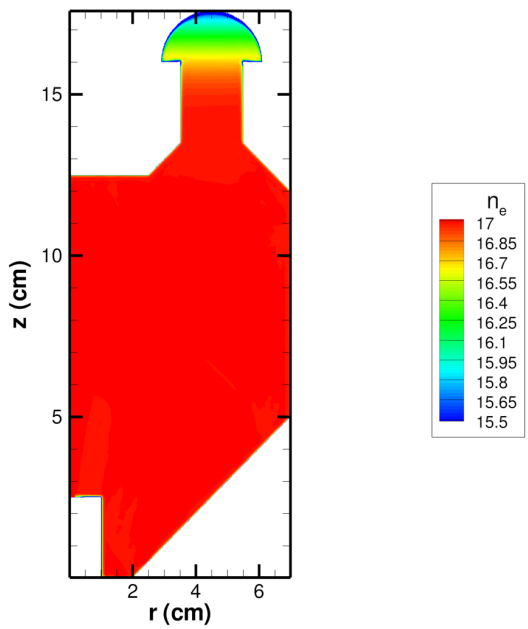

Figure 4.3: Log of electron number density (m^{-3}) after 10 ns.

4.2.2 Initiating Trends

After 100 ns, electrons have now begun to flow from the centre of the discharge chamber towards to the electrode walls. Along their path, they ionize gas particles, increasing ion number density as a result of their collisions. In Figure 4.4, the increase in electron number density can be seen near the electrodes. The reduced mobility of the electrons across the magnetic field has led to a higher density of ion along the field lines. Additionally, ions and and electrons within the acceleration stage are beginning to respond to the electric field by starting to flow outwards (Figure 4.5). Finally, the ion number density is decreasing along the walls of the discharge chamber. There is no secondary emission, meaning electrons which contact the walls are lost. This leads to reduced ion number density along the walls.

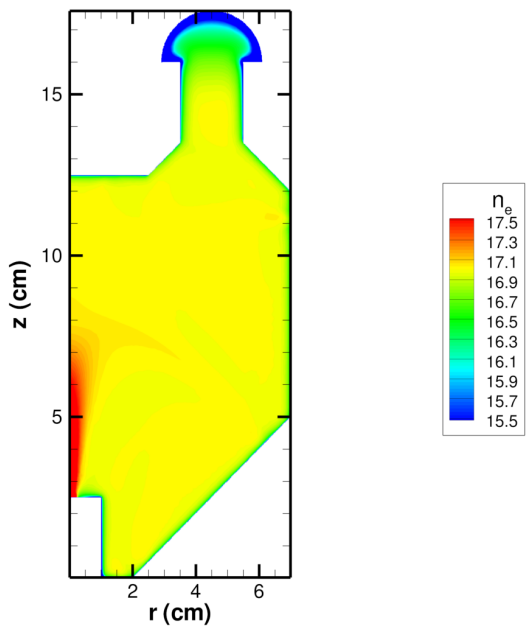

Figure 4.4: Log of electron number density (m^{-3}) after 100 ns.

In Figure 4.5, the electron number density is seen to concentrate along the magnetic field lines. The electrons from the hollow cathode have begun to travel towards the anode walls. Additionally, a small region of higher electron number density is seen at the upper magnetic cusp, nearer the transition region. This further illustrates that the electrons are travelling easily along the magnetic field lines.

After 100 ns, the electrons have begin to noticeably form trends. However, the ions, being much more massive, are slower to respond to the electric fields. They travel much slower and, this being a non-thermal plasma, are at a lower temperature than the electrons.

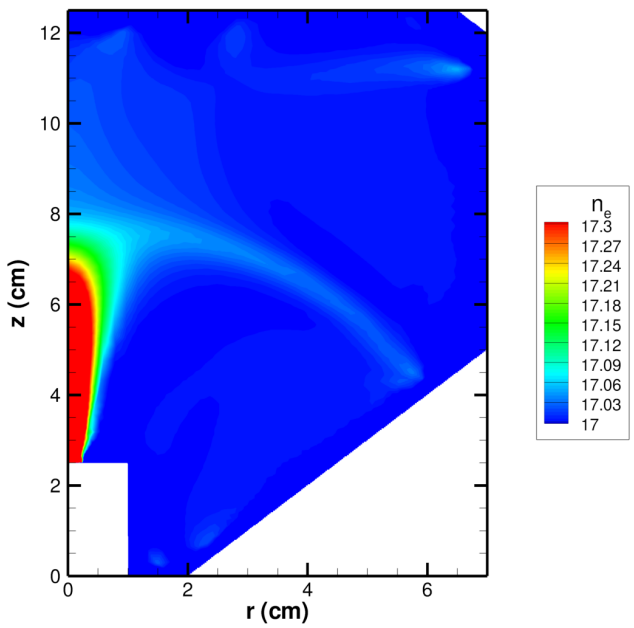

Figure 4.5: Log of electron number density (m^{-3}) after 100 ns. Electrons ejected from the hollow cathode are accelerated towards the anode walls, concentrating along magnetic field lines.

4.2.3 Establishing Steady-State

After 1 μs, the ions have moved through the domain and are approaching steady state. In particular, as seen in Figure 4.6, the ions are forming a beam as they are ejected from the discharge chamber through the acceleration channel. Additionally, the electrons in this region are reaching higher energies due to the high electric field. Along the walls of the acceleration channel, the high magnetic field near the location of the magnet ring impedes electron mobility, reducing densities.

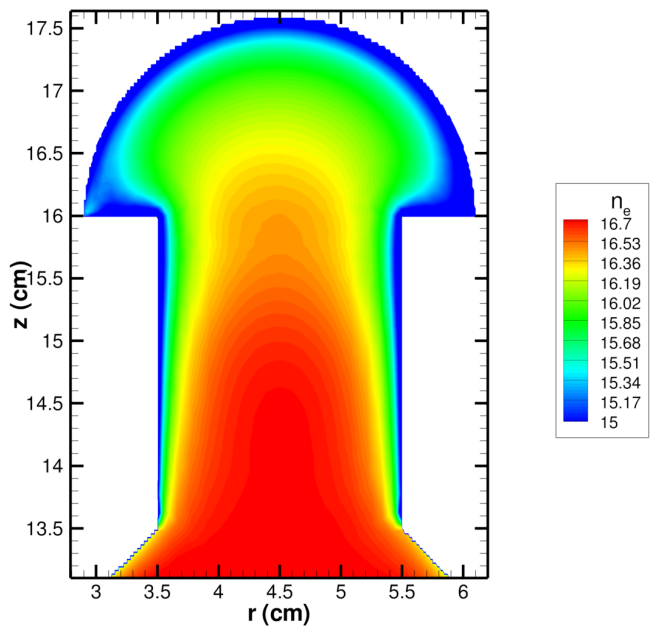

Figure 4.6: Log of electron number density (m^{-3}) after 1 μs within the acceleration stage. Formation of a beam structure is being apparent.

As seen in Figure 4.7, the amplification of the plasma within the discharge chamber due to ionization is reaching its maximum values. Electron densities reach 5×10^{17} m^{-3} in the centre of the discharge chamber. Higher ion number density is being generated at the upper outside region of the discharge chamber. A magnetic cusp is found in this region, allowing electrons to more easily flow outwards towards the walls.

Additionally, some magnetic field lines cross the acceleration zone in this region, due to the strong magnets present at the end of the acceleration channel. These magnetic field lines produce a small barrier to electron flow into the channel. Some impedance to electron flow is useful as it confines electron to the discharge chamber, where they will increase ionization efficiency. However, if the electron current is confined too strongly, ions will be impeded from moving into the acceleration channel.

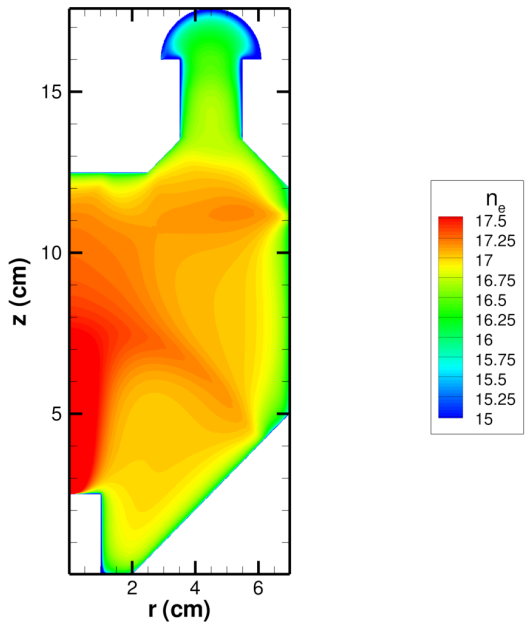

Figure 4.7: Log of electron number density (m^{-3}) after 1 μs. Amplification of the electron number density within the discharge chamber is apparent.

After 10 μs (Figure 4.8) an ion beam is being formed as the ions are ejected from the acceleration channel. Further, the plasma amplification has increased the electron number density within the discharge chamber to 10^{18} m^{-3}. This is close to the steady state value expected for an ion thruster.

At the top of the discharge chamber, near the hub, a small structure is visible in Figure 4.8. This is caused by the magnet which is located on the central hub, along the discharge chamber wall. The hollow cathode directs a jet of electrons almost directly at the hub. Without the magnetic field on the central hub, the electron losses on this portion of the top of the discharge chamber would be very high. The magnetic field here shields the walls here from the electron jet leaving the hollow cathode.

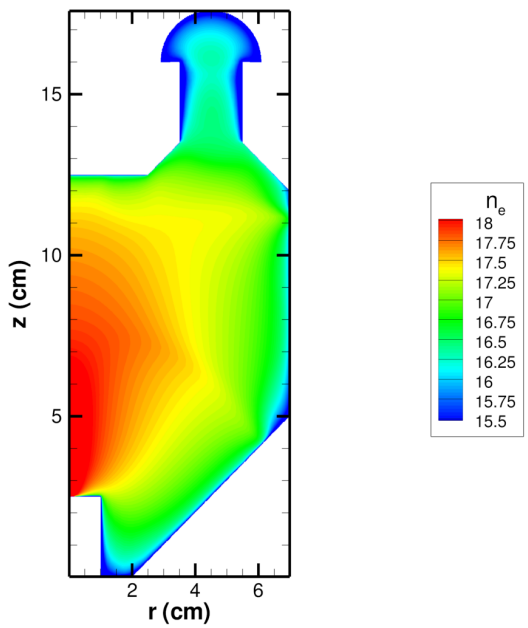

Figure 4.8: Log of electron number density (m^{-3}) after 10 μs. Further amplification of the electron number density within the discharge chamber is visible. Confinement and a beam structure are forming through the acceleration section.

4.2.4 Steady State

After 1 s, all variables have reached steady state and the thruster is functioning as it would in operation. Figure 4.9 shows the electron density through the whole thruster. A peak density of 10^{18} m^{-3} was reached, in line with the ion number densities in similarly sized ion thrusters [2]. Peak ion number densities occurred along the centre line of the discharge chamber, where the hollow cathode injects electrons into the discharge. Ion number density decreases as one moves towards the walls, due to the impeded mobility across magnetic field lines (see Section 2.1.2).

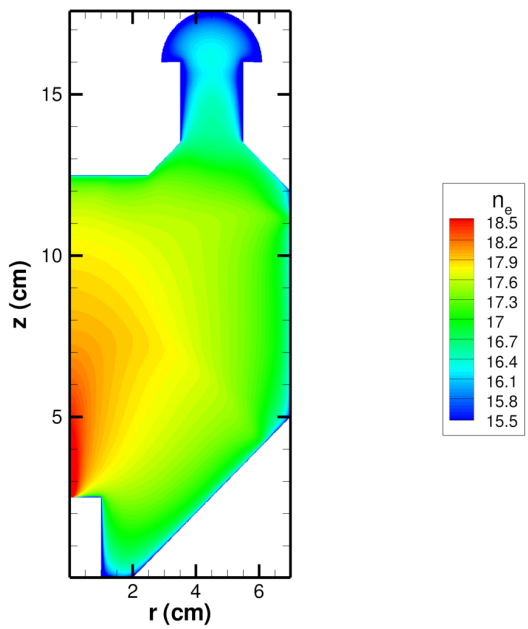

Figure 4.9: Log of electron density (m^{-3}) after 1 s. Steady-state of the system is reached.

Figure 4.10 shows the electron density at various times, taken along a line through the centre of the acceleration channel (see Figure 4.1). As the simulation progresses, the electrons are more and more confined into the discharge chamber. The amplification of the ion number density is apparent as the density increases. Effects of the radial magnetic field of the acceleration stage can be seen as the local maxima found between 14 cm and 16 cm.

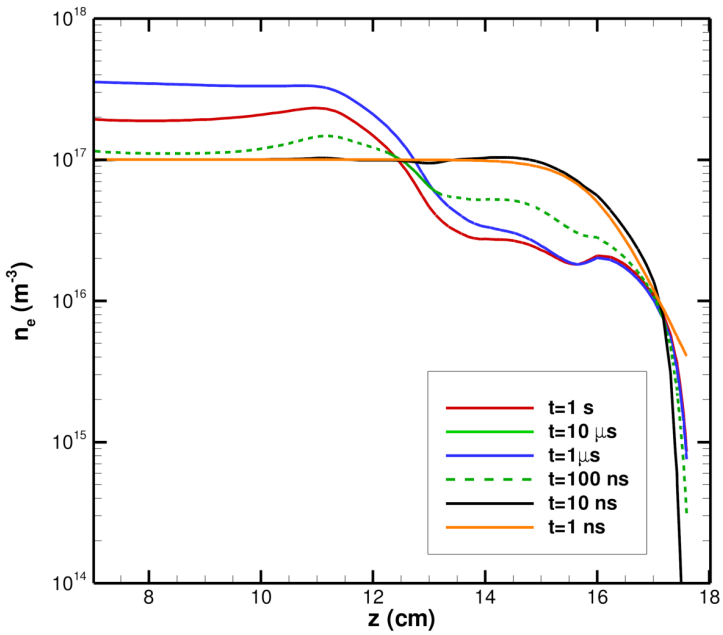

Figure 4.10: Log of electron density (m^{-3}) at various times in the simulation, as found through the centre line of the acceleration stage.

The electric potential within the discharge chamber (Figure 4.11) is relatively flat, decreasing slightly as one moves from the central cathode to the anode walls. Most of the potential drop is captured in the acceleration stage, as expected. Additionally, the potential drop continues outside the acceleration channel. This is a feature found experimentally in Hall thrusters, and is also achieved in the current hybrid design [32]. The electric potential is also drawn down by the dielectric walls within the acceleration channel, as they are not held at a particular potential, and are thus influenced by the exterior ground potential.

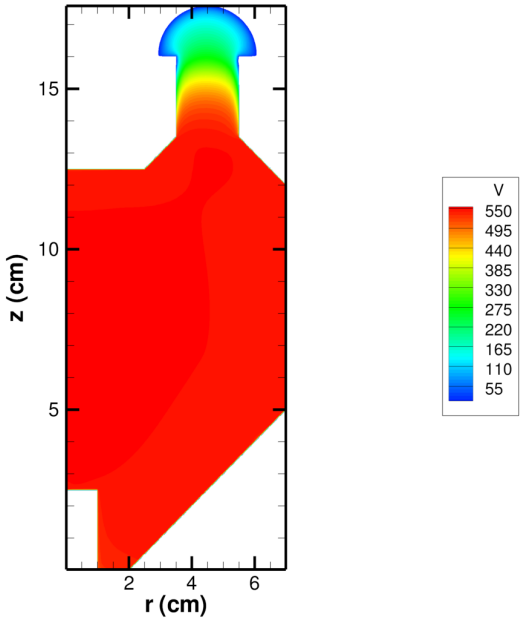

Figure 4.11: Electric potential (V) within the thruster at 1 s.

Electron temperatures within the thruster provides a measure of the average kinetic energy of the electrons (Figure 4.12). This is an important parameter within the thruster, as the ionization rate is highly dependent on it. Within the discharge chamber, electron temperatures are expected to be similar to those found in ion thrusters, around 4 eV [2]. Higher densities are expected where the hollow cathode ejects electrons as these electrons have not lost energy in collisions with neutrals.

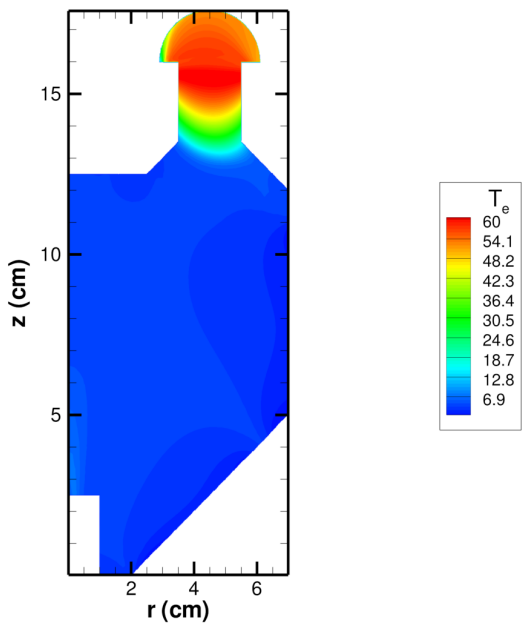

Figure 4.12: Electron temperature (eV) after 1 s through the whole domain.

Results show that the electron temperatures within the discharge chamber are near expected values (Figure 4.13). Differences in the electron temperature may be due to higher energy electrons entering the discharge chamber through the acceleration stage. An exterior hollow cathode is being simulated at the exit boundary in order to neutralize the ejected ion beam. Electrons may leak through the acceleration stage, where they will be accelerated by the applied electric field and enter the discharge chamber at higher energy than the discharge chamber electrons. In a standard gridded ion thruster, few electrons would be leaking into the discharge chamber due to the electric potentials applied by the grids. This means that electrons within an ion thruster are from the hollow cathode or created by ionization, leading to an overall lower electron temperature than would be expected in the hybrid thruster.

The electron temperature is one of the main determinants of the ionization reactions within a plasma discharge. In particular, a higher electron temperature will lead to increased ionization. However, the increased ionization will also create more doubly charge ions. If the electron temperature is too high, the portion of doubly charged ions becomes significant, leading to increased erosion. The higher energy electrons along the central axis mean that the

doubly charged ions will also occur primarily along the central axis. A future hybrid model should investigate the effects of doubly charged ions on the discharge.

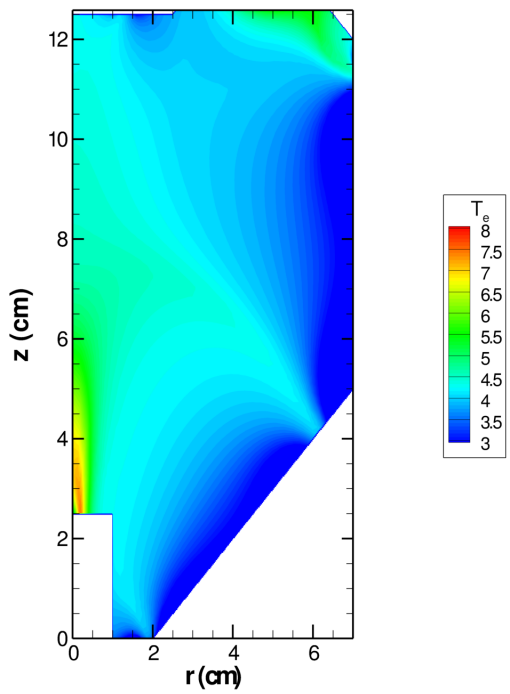

Figure 4.13: Electron temperature (eV) after 1 s in the discharge chamber.

The electrons within the discharge chamber have an electron temperature of 4-6 eV, as shown in Figure 4.13. The lower end of this range is well within expected values [2]. Electron temperatures of 6 eV is higher than expected, but this occurs where the hollow cathode orifice is being simulated. The electric boundary of the orifice is different than the hollow cathode keeper around it, and so the electric field is higher there. This leads to an increased electron temperature right where the orifice injects electrons.

Within the acceleration stage, electrons attained peak values of 60 eV. This is in line with other Hall thrusters, where electron energies are generally found to be 10% of the discharge potential [33]. To summarize, for a Hall thruster with a 300 V discharge potential, peak electron energies will be around 30 eV. In the present case, the discharge potential was 550 V. Additionally, the peak temperature occurs within the acceleration stage, showing proper confinement

of the electrons by the radial magnetic field. As will be explored in Section 4.3, a weaker magnetic field allows the high energy electrons to be pulled outside the thruster.

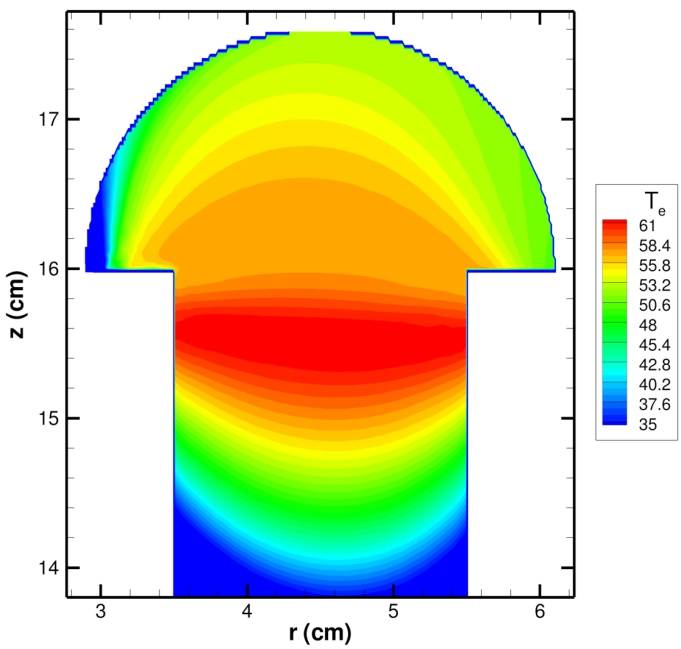

Figure 4.14: Electron temperature (eV) of the acceleration section. The high electric field through the acceleration section leads to substantially higher electron energies than are found throughout the rest of the domain.

Ionization occurs primarily along where the interior cathode ejects electrons, along the field lines and at a lower rate in the acceleration channel (Figure 4.15). This is as expected, with the high ionization rates where high electrons densities occur. In the acceleration region, high ionization rates occur as a result of the high electron energy. Additional ionization in the acceleration stage will produce more ions overall, and lead to less neutral xenon gas being wasted. Any gas which escapes the thruster without being ionized is a major loss in efficiency. The azimuthal Hall current in the acceleration stage provides a second chance for neutral gas particles to be ionized and accelerated by the electric field. Additionally, because ionization in the acceleration stage is lower than in a comparable Hall thruster, the hybrid thruster may not be as prone to the predator-prey oscillations which affect Hall thrusters. Fewer neutrals and decreased ionization may mean that large, unsteady build-ups

of electrons and neutral particles will not occur, or that such oscillations will occur with less amplitude.

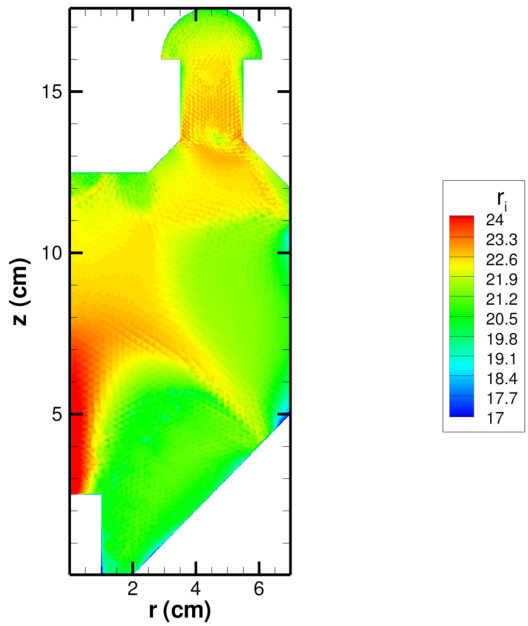

Figure 4.15: Ionization rate ($m^{-3}s^{-1}$) within the thruster at 1 s. Highest ionization regions occur outside the hollow cathode, along magnetic field lines, and through the acceleration channel.

4.2.5 Ion Motion

A vital factor of the steady state hybrid thruster is the formation of an ion beam. Ions are drawn from the discharge chamber, through the acceleration stage and ejected out of the thruster. Figure 4.16 shows the ion velocity magnitude with streamlines delineating the path of the ions.

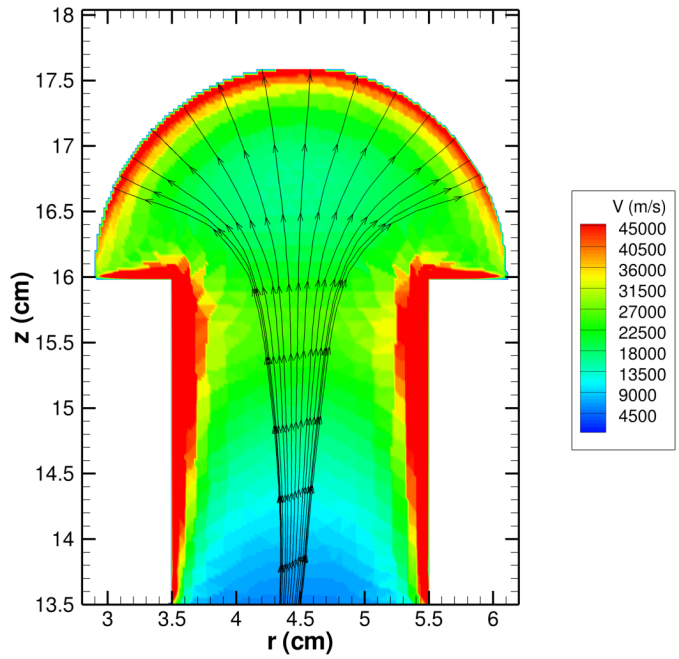

Figure 4.16: Ion velocity magnitude through the acceleration channel, with streamlines denoting flow.

Ion velocities are within expected ranges (discussed further in Section 4.5), peaking where electric field strength is highest. Ion velocity can also be seen to increase rapidly near the channel walls. This is due to charge build-up on the simulated dielectric walls within the acceleration channel. The high velocity regions near the walls are a concern for erosion. As will be discussed further in Section 5.2, magnetic shielding may be helpful in reducing wall erosion.

From the streamlines, it is clear that there is a beam divergence occurring. The central, high density region the beam does exit in the axial direction, but ions which are not on the centreline are directed with large radial components. It is important to note that this may, in part, be caused by the curved exit boundary. The exit boundary is held at ground potential, strongly attracting the ions as they leave the acceleration channel. The curved boundary was used to try and match the shape of the magnetic field lines in this area. Electric potential tends to be constant along magnetic field lines, as electrons can more easily flow along lines than across, and so the charge is negated more easily along lines.

4.3 Magnetic Field Optimization

As discussed previously, a magnetic field is important in both Hall and ion thrusters. In Hall thrusters, a strong radial magnetic fields generates the a Hall current in the azimuthal direction. This provides strong confinement of the electrons, allowing high ionization rates and helping to establish the accelerating electric field. In an ion thruster, a magnetic field is established such that the magnetic field lines are primarily parallel with the discharge chamber walls. Electron mobility is greatly reduced across magnetic field lines, and so this magnetic field configuration reduces electron losses to the walls.

4.3.1 Modified Magnetic Field

In the hybrid thruster, particular interest is given to the magnetic field as the configurations of both ion and Hall thruster must be smoothly combined. To accomplish this, an additional ring of magnets was added at the interface between the ionization chamber and the acceleration stage. The extra ring of magnets establishes a radial magnetic field in the opposite direction to the existing acceleration stage magnetic field (shown in Figure 4.17). The additional ring of magnets creates a weak magnetic field in the transition region [34, 35]. This creates a low field cusp between the two rings of magnets (Figure 4.18), where electrons may travel without significant resistance. If electrons can easily flow into the channel through this low field region, the unmagnetized ions should be attracted along to equalize the space charge. Additional ions in the acceleration raises the thrust by increasing the overall mass flow.

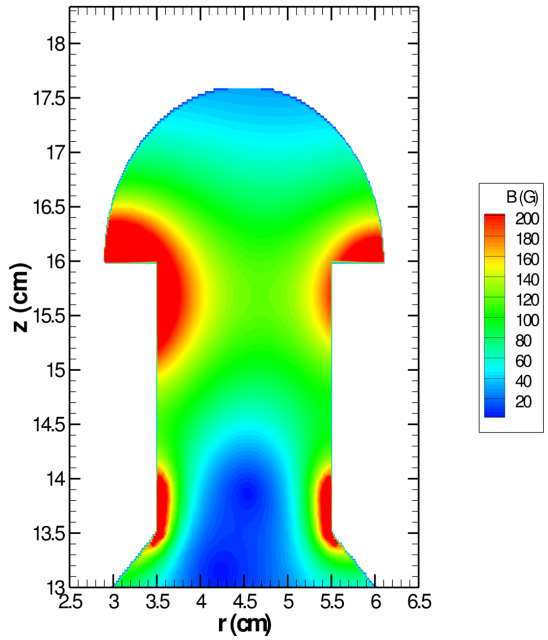

Figure 4.17: Radial magnetic field strength (G) within the hybrid thruster after the addition of a second ring of magnets through the acceleration channel.

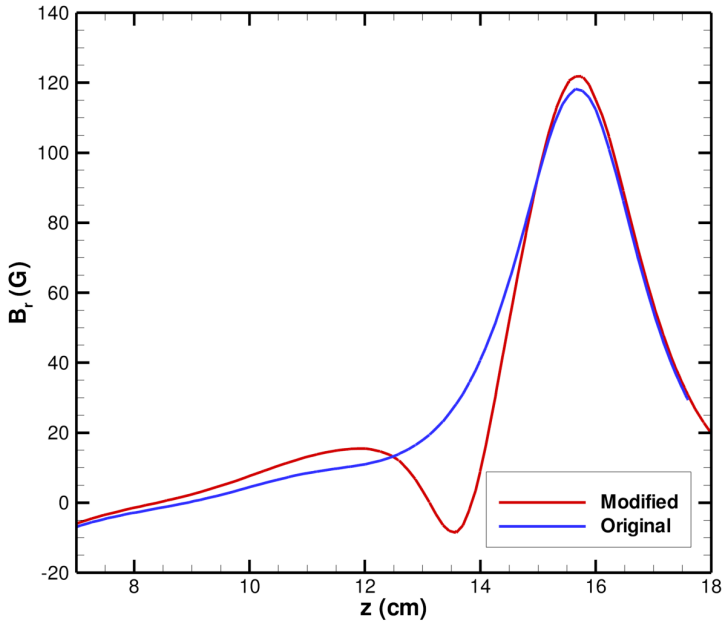

Figure 4.18: Radial magnetic field strength (G) within the hybrid thruster after the addition of a second ring of magnets through the acceleration channel.

Figure 4.19 shows the electron density through the thruster domain with the modified magnet structure. A small cusp is apparent in the acceleration stage, though the electron density is lower with the modified magnet structure than the original further along the channel. This is caused by a stronger magnetic field at the end of the acceleration stage. These extra rings of magnets direct the field in the opposite direction of the original radial magnetic field in the acceleration channel. However, near the end of the acceleration channel, this means that the field lines created by the newly added rings, are in the same direction as the magnetic field created by the original ring magnets. This has the effect of boosting the radial magnetic field in the area of the region of the original magnetic field.

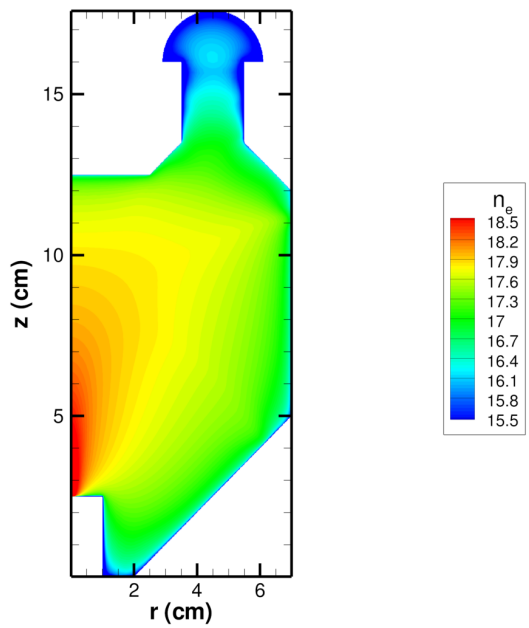

Figure 4.19: Log of electron density (m^{-3}) after 1 s with an additional ring of magnets in the acceleration stage.

A comparison of the electron density along the centreline of the acceleration stage between the two magnet configurations is shown in Figure 4.20. The densities are increased through the discharge chamber, but decreased through the acceleration channel. The extra ring of magnets impeded electron motion into the acceleration stage. By keeping electrons in the discharge stage, densities are increased, with the trade off of lower densities in the acceleration stage.

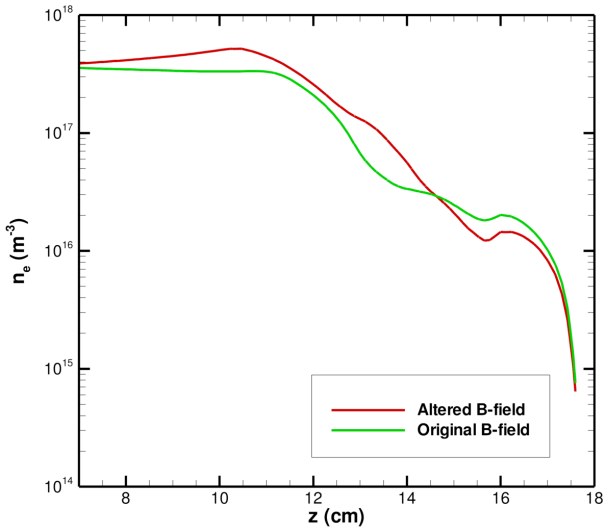

Figure 4.20: Electron density (m^{-3}) along the centreline of the acceleration stage after 1 s, as compared to the results for the unaltered magnetic field case.

The energy and behaviour of electrons within the thruster is strongly dependent on the magnetic field. The stronger magnetic field in the latter portion of the acceleration stage had the effect of boosting the electron temperature. This was due to a higher electric field, as the electrons were firmly confined by the stronger magnetic field.

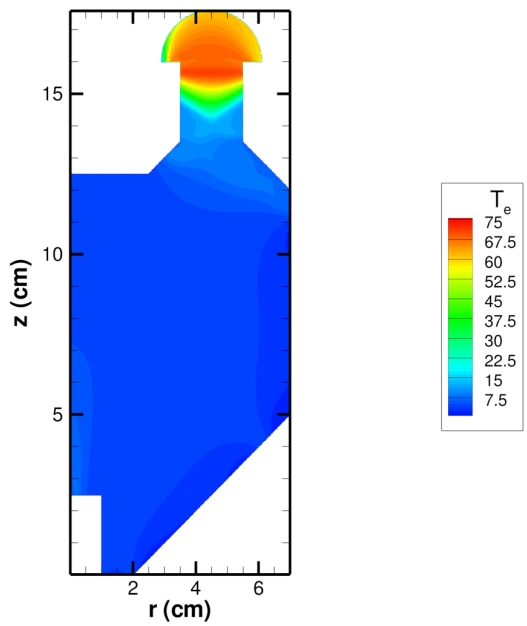

Figure 4.21: Electron Temperature (eV) after 1 s for the altered magnetic field hybrid thruster.

Altering the magnetic field in the acceleration stage has created a higher electric field, raising the electron temperature (Figure 4.21). Interestingly, this also increases the ion velocity (discussed further in Section 4.5).

4.3.2 Magnetic Field Strength

The magnetic field in the acceleration stage is important to the effective function of the hybrid thruster. The interaction of the electric and magnetic fields are responsible for confining the electrons and accelerating the ions. For this reason, a range of magnetic field strengths were tested, with specific attention given to how this affected plasma behaviour within the acceleration stage.

Figure 4.22 shows the electron temperature through the acceleration channel in four different simulations. Each simulation has a different selected magnetic field strength in the acceleration channel. As the magnetic field strengthens, the electrons are more tightly confined, as expected. The electrons caught in the acceleration channel create the axial electric field used to accelerate the ions. If the electrons are weakly confined, they can move outside the channel. Once outside, the electric field created between the electrons

and the neutralized ion beam is able to gain radial components, as the walls of the channel no longer restrict the electric field to be primarily in the axial direction. The additional radial components contribute to increased beam divergence and reduced thruster efficiency.

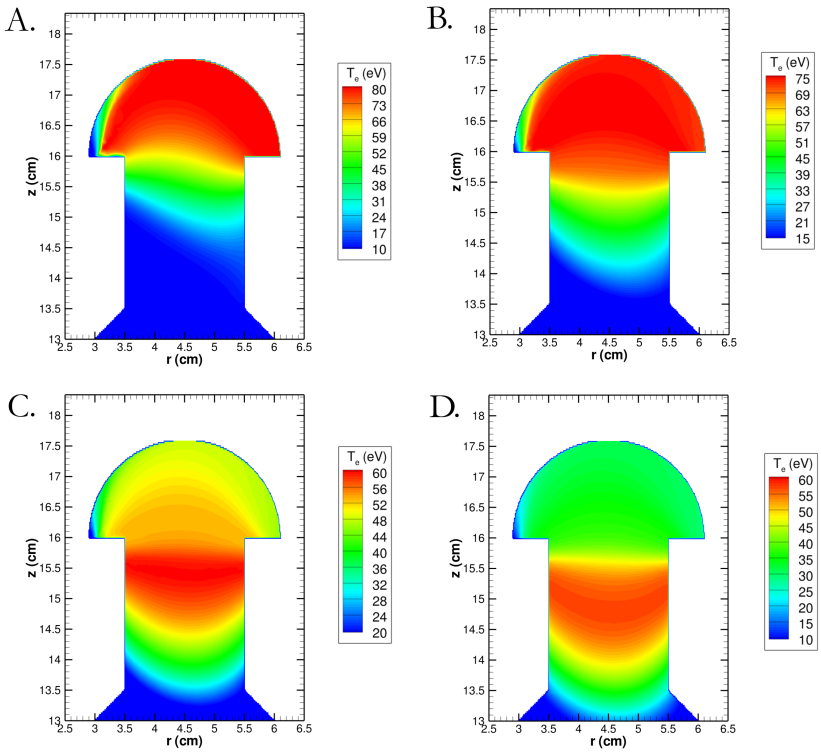

Figure 4.22: Electron temperature for various magnetic field strengths, here denoted by the peak radial field strength for each case. A) 12 G B) 59 G C) 130 G D)180 G

The optimal magnetic field should be strong enough to confine the electrons within the acceleration channel. However, a stronger field will require more power, and so attention must be given to keeping the field as weak as possible.

4.4 Electric Potential Optimization

One of the primary reasons for creating the hybrid thruster is to increase the acceleration potential used in Hall thrusters. A higher potential increases the specific impulse, leading to more fuel efficient operation. Currently, Hall thrusters are limited in the acceleration potential used by plasma instabilities. The plasma instabilities reduce the functioning stability of the thruster. To test the effects of increased potential, a range of acceleration potentials was modelled.

Figure 4.23 shows the electron temperature in the acceleration channel for four different electric potentials. As the electric potential increases, the electron density increases proportionally. Additionally, the stronger electric field pushes the peak electron density outside of the acceleration channel. The movement of the peak electron temperature outside of the acceleration channel demonstrates that the magnetic field is no longer strong enough to impede the axial mobility of the high energy electrons.

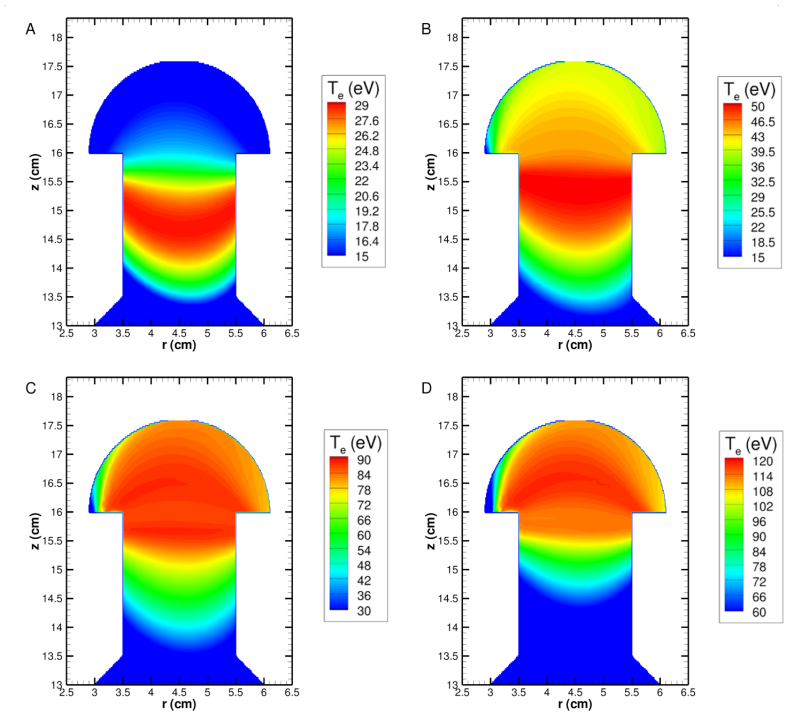

Figure 4.23: Electron temperature within the acceleration stage after 1 s, for 4 different potentials. A) 245 V, B) 445 V, C) 745 V, D) 945 V.

A related trend can be seen in Figure 4.24, which shows the ion density through the acceleration stage for a sweep of discharge potentials. As the potential increases, the ion number density within the discharge chamber increases. However, the ions are also ejected from the acceleration stage at a faster rate. This in turn lowers the density of the ion beam. To increase the density within the beam, and so increase the thrust, the magnetic field should be correspondingly increased to better confine the electrons. This should lead to an increase in the ion number density as well, due to forces arising to maintain quasi-neutrality.

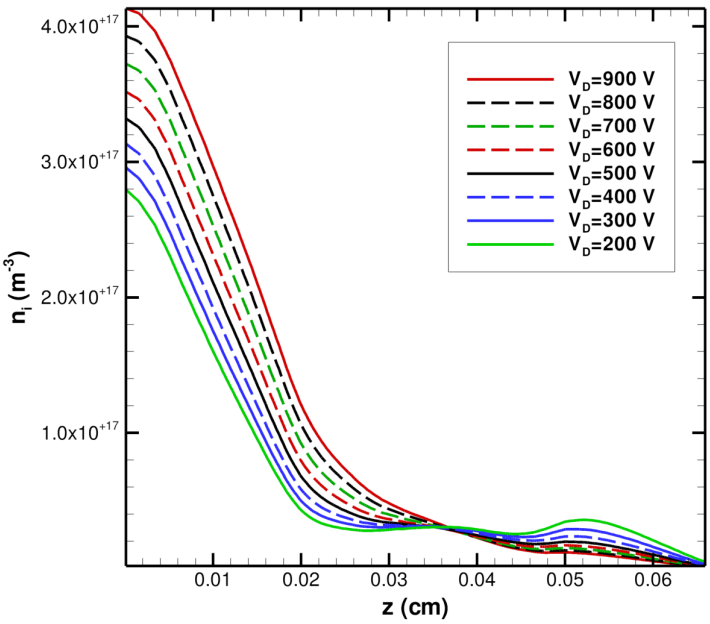

Figure 4.24: Ion density taken along a line through the centre of the acceleration stage for various discharge potentials.

The electrons confined within the acceleration channel are largely responsible for creating the electric field which drives ions out of the thruster. If the electrons are moving outside the channel, the electric field ends up being curved. Instead of being purely axial, the electric field takes on radial components, increasing beam divergence and reducing efficiency.

4.5 Thruster Performance

In order to evaluate the performance of the thruster, global parameters were calculated. Specific impulse was calculated by integrating over the exit plane of the thruster to determine the average exist velocity. Equation 1.2 then gives the specific impulse. To calculate the total thrust, the velocity and mass flow rate were multiplied, and integrated over the exit plane (see Equation 4.1). In particular, thrust and specific impulse are used to compare the thruster to other thruster designs. Thrust in the hybrid thruster was calculated to be 8.4 mN, while the hybrid thruster with the modified magnetic field had a thrust of 8.0 mN. The specific impulse of the two configurations were 1340 s and 1640

s, respectively. The higher thrust but lower specific impulse of the unmodified thruster is due to the effects the different magnetic fields in each version. The modified magnetic field structure had the unintended consequence of increasing the magnetic field through the later part of the acceleration channel. The increased magnetic field confined the electrons more tightly. This leads to a higher electric field, which accelerates the ions to higher velocities and so higher specific impulse. However, the density of the accelerated beam is lower, leading to less overall mass flow and lower total thrust.

$$H = \int_S \vec{v} \dot{m} dS \tag{4.1}$$

Table 4.1 shows the performance of the hybrid thruster compared to similar ion or Hall thruster. The hybrid thruster shows performance generally in agreement with thrusters in a similar power range. The hybrid thruster operates at roughly 1.4 kW. The primary deviation from expected values comes from the thrust, which is significantly lower than expected. This is the result of the lower ion number densities within the acceleration channel. Low ion number densities within the acceleration channel lead to decreased beam currents and overall mass flux out of the thruster. In the hybrid thruster, ion number density through the acceleration stage are of the order 10^{16} m^{-3}. Ideally, these densities would be greater than 10^{17} m^{-3}. Moreover, boundary conditions used in this simulation may be causing a decrease in the particle number densities in the ion beam. As shown in Figure 4.10, the particle densities drop rapidly near the exit boundary, likely lowering the density through the plume region. Future work should focus on optimizing the conditions which would lead to an increase of the ion densities within the thruster, especially the acceleration channel, hence create larger beam currents.

Table 4.1: Examples of Hall and ion thruster with specific impulse and thrust compared to the hybrid thruster. Note that the power of these thrusters ranges between 1-3 kW.

	Type	**Thrust (mN)**	**Specific Impulse (s)**
NASA-173GT	Hybrid	90	1800
NSTAR	Ion	62	3070
HEMP-T	HEMP	57	3000
SPT-100	Hall	98.8	1876
PPS-1350-G	Hall	90	1660
Hybrid	Hybrid	8.0	1340
Hybrid (modified)	Hybrid	8.4	1640

4.6 Concluding Remarks

A hybrid thruster model was created and simulations run to understand underlying phenomena and determine performance. Specifically, the evolution of the plasma with thruster was studied, with trends being in agreement with other ion and Hall thrusters [2, 36]. The higher temperature electrons within the discharge chamber are confined by the magnetic field cusp structure. This leads to increased ionization along the central axis. Within the Hall portion, the radial magnetic field and the axial electric field together produce an azimuthal Hall current of electrons. Travelling in the azimuthal direction lengths the residence time and collision probability of the electrons in the acceleration stage, leading to increased ionization. While the ionization is intended to occur primarily in the discharge chamber, any additional ionization in the Hall-like acceleration stage will increased the propellant utilization efficiency. More xenon will be ionized, leading to overall greater thrust.

The space-time evolution of the plasma within the thruster is summarized hereafter. The initiation of the discharge begins with electrons being ejected from the hollow cathode at approximately 10 ns. These energetic electrons start to ionize neutral gas atoms, creating additional electrons. As the plasma continues to increase in density, at approximately 1 μs, electrons begin to drift towards the anode walls along the magnetic field lines. Ion number density increase due to the electron collisions in the discharge chamber. Electron motion is impeded by magnetic field lines, restricting their motion towards the walls, as shown by electrons concentrating along field lines. As ions accumulate within the discharge chamber, the electric field in the acceleration channel begins to draw ions out of the discharge chamber, forming an ion beam. Simultaneously, electrons are drawn into the acceleration region from the external neutralizing cathode. Moreover, high temperature electrons accumulate near the exit plane due to the accelerating electric fields. The external boundary is held at ground potential, which, along with the magnetically confined electrons, establishes a high electric field. Ion ejection through the acceleration channel occurrs as the simulation settles into steady state. The discharge potential and magnetic field strength were varied to study the plasma behaviour and optimize the thruster. As expected, increasing the magnetic field more effectively confines the electrons within the acceleration channel. Additionally, an altered magnetic field structure was tested and evaluated on its performance. The altered magnetic field structure increases the electric field strength and consequentially I_{sp}. However, the additional ring of magnets reduces the amount of ions flowing into the acceleration channel, reducing total thrust. All the results are insightful in understanding the behavoir of the

hybrid thruster. Recommendations and conclusions will be further discussed in the final chapter.

5 Summary and Concluding Remarks

5.1 Conclusions

Electric propulsion (EP) technology offers advantages over conventional chemical thrusters for specific space mission applications. The high specific impulse of EP allows for large changes in spacecraft velocity using relatively small amounts of propellant. Increased propellant efficiency allows for reduced missions costs or extended mission capabilities. Developments in power systems and successful landmark missions have increased the usage of EP aboard commercial satellites. Further, growing interest in using swarms of smaller satellites provides an attractive application for the precise, low noise thrust of EP.

Hall and ion thruster are two of the most commonly used electrostatic thrusters. Both offer particular advantages derived from their different methods of operation. In particular, Hall thrusters are able to generate greater thrust due to their lack of grid electrodes at the exit. In contrast, ion thrusters can stably operate at higher discharge potentials, leading to higher specific impulse (ion velocities). A hybrid Hall-ion thruster was designed and evaluated to test whether advantages of each system may be leveraged to create an EP device with improved performance. To test the conceptual design, a model was created using multiphysics time-dependent simulation software. Optimization of various parameters was undertaken to increase performance and understand the details of the underlying phenomena.

Figure 5.1 shows the hybrid thruster, with key temporal and spatial trends indicated. The initiation of the thruster begins with the ejection of electrons from the hollow cathode (Region A in Figure 5.1) into the centre of the discharge chamber. Soon after, electrons are seen streaming towards the anode walls (Region B), following magnetic field lines. As electrons are accelerated

towards the anode walls, neutral gas particles are ionized, amplifying the discharge (Region C). Ions accumulate within the discharge chamber, eventually drifting towards the acceleration channel (Region D). Ions are accelerated by the potential maintained by the axially confined electrons (Region E). The ions extracted from the discharge chamber and ejected through the acceleration channel at high velocity form the ion beam (Region F).

Simulation results indicate that thruster performance is in line with expectations based on other EP technology. Electron and ion motion within the hybrid thruster are in agreement with expected results, based on Hall and ions thrusters. While the hybrid device is not directly comparable to existing EP thruster models, examining the plasma behaviour and evolution within Hall and ion thrusters separately allows for some comparison to be made. In particular, the plasma number density at steady-state within the discharge chamber is as expected from experiments. The similarly sized NSTAR thruster has a peak electron density of 2.5×10^{18} m^{-3}, directly outside the hollow cathode. The hybrid thruster reaches a similar peak electron number density outside the hollow cathode, decreasing towards the anode walls [37]. Additionally, the electron temperature within the hybrid thruster is in close agreement with measured values from the NSTAR thruster. [37]. Further, moving into the acceleration channel, the electron temperature is near the expected value of a Hall thruster, at roughly 10% of the discharge potential. As in a Hall thruster, high temperature electrons are found along the exit plane, where the high accelerating electric fields are present [38]. The total thrust and specific impulse are within the range of expected values for thrusters in the 1-2.5 kW range. The thrust is on the lower range of expectations, however, this is due to the fact that the plasma number density in the acceleration channel and consequently ion beam is below that of conventional Hall thrusters. If the plasma number density is increased to expected values, the total thrust will be competitive with modern thrusters. The time-dependant simulations are insightful in understanding the behaviour of the hybrid electric propulsion system.

The hybrid thruster is a new proposed design which will require further iterations and study before its potential may be determined. The low thrust of the device at its present stage may lead one to conclude that the design is no longer worth pursuing. However, the design and modelling of the thruster is still in its early stages. Future work should be able to identify the cause of the lower ion number density within the acceleration channel. Once the cause of the low ion number density is identified, and the problem corrected, the hybrid thruster presents potential advantages. Operating without grids at a high potential would allow for a high specific power thruster able to attain the

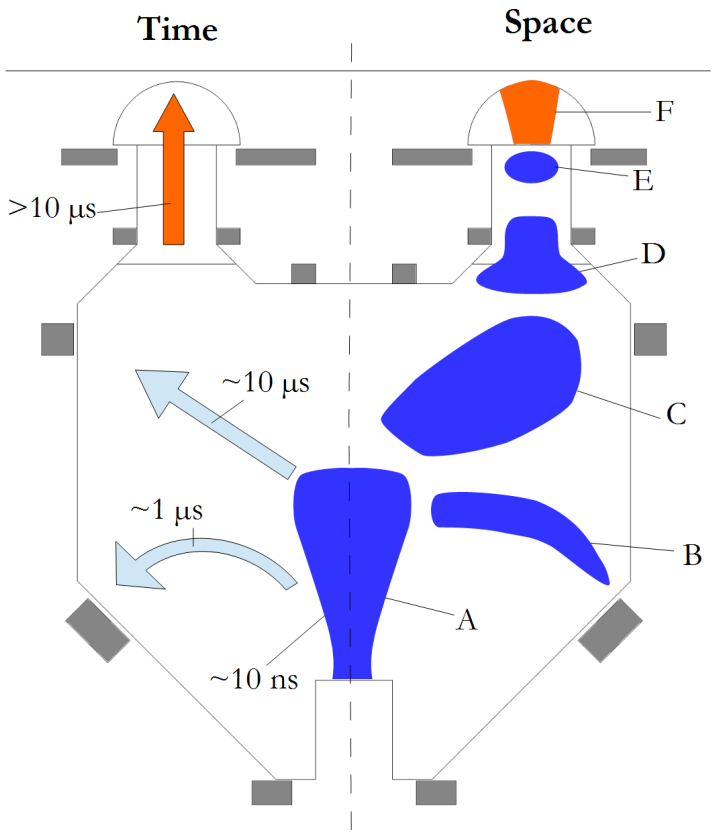

Figure 5.1: Diagram of the hybrid thruster with key temporal moments and spatial locations noted. Blue denotes primarily electron dynamics, while orange represents ion dynamics. A) Hollow cathode ejects electrons into the discharge chamber, igniting the plasma. B) Reduced plasma density near walls due to impeded electron motion across field lines. C) Ions drift towards the acceleration stage. D) Ions flow into the acceleration channel, though particle flow is hindered by the addition of a an extra ring of magnets. E) Electrons along the exit plane reach high energies along the radial field lines due to high acceleration electric fields. F) Ions are ejected and accelerated by strong axial electric fields, forming the ion beam.

high exhaust velocity of an ion thruster. This would allow expanded mission capabilities, shoter mission durations, and decreased mission costs due to fuel savings. For these reasons, the hybrid thruster warrants further investigation.

5.2 Future Considerations and Recommendations

The hybrid thruster modelled here shows performance in line with expectations, however, future work will help to increase thruster performance. Several recommendations that could be implemented in the formalism and physical model to devlop the understanding of the hybrid thruster are discussed.

On the computational side, the use of particle-based or hybrid method to model the simulation would be beneficial in validating the hybrid thruster results [39]. The hybrid thruster combines plasmas of different types, each often modelled using distinct methods. This means that modelling the entire hybrid thruster domain using a fluid based method may be testing some of the approximations. A particle or hybrid method would allow the results to be approached from a different angle, lending support or showing where inaccuracies may be found.

Further, the present work is limited by the axisymmetric method used. In reality, the hybrid thruster is likely to have unsteady plasma processes. Particularly, oscillations in the azimuthal direction. Hall thrusters exhibit azimuthal plasma oscillations, and these would likely be present in the hybrid thruster as well [40]. Plasma oscillations represent a major source of inefficiency in an EP device, and so determining their effect on the hybrid thruster is important. A full 3D model would be ideal to study the azimuthal oscillations, as well as more accurately gauge the effects of structural components which could not be included in the axisymmetric study. Specifically, the supports which hold the central hub of the thruster in place will increase electron losses in the discharge chamber, and so their effect needs to be understood.

An additional area for future improvement is along the external boundary, where the ion beam exits the simulation. Along the external boundary, a ground potential is applied. This creates a region of extremely high electric field, causing space charge separation. This region of high electric field and space charge accelerates the nearby ions to unrealistic speeds. In future models, this boundary conditions should be refined to reduce the artificially created space charge along the external boundary. One approach to accomplish this is to model a larger region of the plume, allowing the neutralizing cathode electrons to more accurately shape the electric field outside the thruster. However, care must be taken as the pressure outside the thruster is low, and

careful consideration must be given to the modelling method used. In particular, the electron mobility in the plume is drastically different in value than in the acceleration channel. Additionally, the external boundary leads to greatly reduced number densities. This likely leads to unrealistically low thrust measurements. Refinement of the boundary condition may lead to more accurate modelling and improved performance.

Erosion is the primary lifetime limiting phenomena in both Hall and ion thruster [41, 42]. The hybrid thruster does not have the acceleration grids of an ion thruster, and so this erosion method is avoided. However, the hybrid thruster does have the discharge channel of a Hall thruster. The channel walls are subject to high energy bombardment by plasma particles. This causes sputtering of the material, and eventual failure. To combat this, recent Hall thruster designs have used an altered magnetic field configuration [7, 43]. The outer magnet ring is angled in such a way as to direct the field lines around the outer channel wall. High energy electrons are largely responsible for the outer wall erosion. These electrons flow along the field lines, that conventionally would intercept the outer channel wall. By angling the outer magnet ring, the field lines do not intercept the channel wall, and so the erosion rates are greatly reduced.

Additionally, temperature effects on neutral gas particles may offer additional gains in efficiency. Though the hybrid thruster operates at low pressures, there will be some heating of neutral gas particles due to collisions with more energetic ions. Heated neutral gas is able to generate thrust, as seen with conventional chemical rockets. If the hybrid thruster heats gas particles to a high degree, the hybrid thruster may be able to function effectively in an electrothermal mode. To leverage electrothermal heating, design alterations would need to be made to confine and efficiency expand the heated gas. However, an investigation of this possibility may prove useful.

Finally, there is great interest in the use of EP technology for micro and nano-satellites [44, 45]. To be used on such small platforms, EP devices must be scaled in power and size. An investigation to determine the effects of scaling the hybrid thruster down would be valuable in evaluating its potential application for nano-satellites.

Bibliography

[1] George P. Sutton and Oscar Biblarz. *Rocket Propulsion Elements*. Wiley-Interscience, seventh edition, 2001.

[2] Richard E. Wirz. *Discharge plasma processes of ring-cusp ion thrusters*. PhD thesis, California Institute of Technology, 2005.

[3] Michael McDonald, Christopher Bellant, Brandon St. Pierre, and Alec Gallimore. Measurement of Cross-Field ElectronCurrent in a Hall Thruster Due to Rotating Spoke Instabilities. *47th AIAA/ASME/SAE/ASEE Joint Propulsion Conference & Exhibit*, AIAA 2011-5810, 2011.

[4] V. A. Lisovskiy and S. D. Yakovin. Experimental study of a low-pressure glow discharge in air in large-diameter discharge tubes: I. conditions for the normal regime of a glow discharge. *Plasma Physics Reports*, 26(12):1066–1075, 2000.

[5] PY Peterson. *The development and characterization of a two-stage hybrid hall/ion thruster*. PhD thesis, The University of Michigan, 2004.

[6] Daren Yu, Maojiang Song, H. Liu, Y. J. Ding, and Hong Li. Particle-in-cell simulation of a double stage Hall thruster. *Physics of Plasmas*, 19(3):033503, 2012.

[7] Ryan W. Conversano, Dan M. Goebel, Richard R. Hofer, Taylor S. Matlock, and Richard E. Wirz. Magnetically Shielded Miniature Hall Thruster: Development and Initial Testing. *33rd International Electric Propulsion Conference*, IEPC-2013-201, 2013.

[8] G. J. M. Hagelaar, J. Bareilles, L. Garrigues, and J.-P. Boeuf. Role of anomalous electron transport in a stationary plasma thruster simulation. *Journal of Applied Physics*, 93(1), 2003.

[9] Ulrich Walter. *Astronautics: The Physics of Space Flight*. Wiley-VCH, 2012.

[10] Edgar Choueiri. A Critical History of Electric Propulsion: The First Fifty Years (1906-1956). *40th AIAA/ASME/SAE/ASEE Joint Propulsion Conference and Exhibit*, AIAA-2004-3334, July 2004.

[11] Robert G Jahn and Edgar Y Choueiri. *Electric Propulsion*, volume 5. Academic Press, third edition, 2002.

[12] M. Andrenucci, F Paganucci, P. Rossetti, V. Antoni, G. Serianni, M. Bagatin, C.a. Borghi, A. Cristofolini, A. Cristofolini, and R. Ghidini. Magneto-Plasma-Dynamic Thrusters for Space Applications. *33rd Plasmadynamics and Lasers Conference*, AIAA 2002-1113, 2002.

[13] John R. Brophy. NASA's Deep Space 1 ion engine. *Review of Scientific Instruments*, 73(2), 2002.

[14] Michael Sean MacDonald. *Electron transport in Hall Thrusters*. PhD thesis, The University of Michigan, 2012.

[15] Hans J Leiter, Rainer Killinger, Helmut Bassner, Johann Muller, and Ralf Kukies. Development of the Radio Frequency Ion Thruster RIT XT: A Status Report. *27th International Electric Propulsion Conference*, IEPC-01-104, 2001.

[16] Cristina Bramanti, Roger Walker, and Orson Sutherland. The Innovative Dual-Stage 4-Grid Ion Thruster Concept: Theory and Experimental Results. *57th International Astronautical Congress*, IAC-06-C4.4.7, 2006.

[17] CC Farnell. *Performance and lifetime simulation of ion thruster optics*. PhD thesis, Colorado State University, 2007.

[18] F. S. Gulczinski and R. A. Spores. Analysis of Hall-effect thrusters and ion engines for orbit transfer missions. *32nd Joint Propulsion Conference and Exhibit*, AIAA 96-2973, 1996.

[19] JR Brophy and RY Kakuda. Ion propulsion system (NSTAR) DS1 technology validation report. *JPL Publication 00-10*, 2000.

[20] C H Edwards, N C Wallace, C Tato, and P van Put. The T5 Ion Propulsion Assembly for Drag Compensation on GOCE. *Second International GOCE User Workshop*, (ESA SP-569), 2004.

[21] Mark R Drinkwater, R Haagmans, D Muzi, A Popescu, R. Floberghagen, M. Kern, and M. Fehringer. THE GOCE GRAVITY MISSION: ESA'S FIRST CORE EARTH EXPLORER. *3rd International GOCE User Workshop*, SP-627, 2006.

[22] B. H. Foing, G. D. Racca, A. Marini, D. J. Heather, D. Koschny, M. Grande, J. Huovelin, H. U. Keller, A. Nathues, J. L. Josset, A. Malkki,

W. Schmidt, G. Noci, R. Birkl, L. Iess, Z. Sodnik, and P. McManamon. Smart-1 mission to the moon: Technology and science goals. *Advances in Space Research*, 31(11):2323–2333, 2003.

[23] Chen Juanjuan, Zhang Tianping, Liu Mingzheng, and Jia Yanhui. PIC/MCC Simulation Computational Modeling of a Ion Thruster Discharge Chamber. *33rd International Electric Propulsion Conference*, IEPC-2013-162, 2013.

[24] G J M Hagelaar, J Bareilles, L Garrigues, and J.-P. Boeuf. Modelling of Stationary Plasma Thrusters. *Contrib. Plasma Phys.*, 5-6:529–535, 2004.

[25] Yoshiro Arakawa and P. J. Wilbur. Discharge plasma calculations in cusped ion thrusters using the Finite Element Method. *20th International Electric Propulsion Conference*, IEPC 88-079, 1988.

[26] V. A. Lisovskiy, V. A. Koval, E. P. Artushenko, and V. D. Yegorenkov. Validating the Goldstein–Wehner law for the stratified positive column of dc discharge in an undergraduate laboratory. *European Journal of Physics*, 33(6):1537–1545, 2012.

[27] Fabrizio Garulli, Andrea and Giannitrapani, Antonio and Leomanni, Mirko and Scortecci. Autonomous Low Earth Orbit Station-Keeping with Electric Propulsion. *Journal of Guidance, Control, and Dynamics*, 34(6):1683–1693, 2011.

[28] G Kornfeld, N Koch, and HP Harmann. Physics and evolution of HEMP-thrusters. *30th International Electric Propulsion Conference*, IEPC-2007-108, 2007.

[29] Tim Brandt, Rodion Groll, Frank Jansen, and U Johann. Magnetohydrodynamics and particle-in-cell codes simulation of plasma processes in micro HEMP-Thrusters. *33rd International Electric Propulsion Conference*, IEPC-2013-145, 2013.

[30] Cross sections extracted from Program Magboltz, Version 8.9 March 2010, 2014.

[31] G J M Hagelaar and L C Pitchford. Solving the Boltzmann equation to obtain electron transport coefficients and rate coefficients for fluid models. *Plasma Sources Science and Technology*, 14:722–733, 2005.

[32] Justin W. Koo and Iain D. Boyd. Modeling of anomalous electron mobility in Hall thrusters. *Physics of Plasmas*, 13(3):033501, 2006.

[33] James M Haas. *Low-Perturbation Interrogation of the Internal and Near-Field Plasma Structure of a Hall Thruster Using a High-Speed Probe Positioning System.* Phd. dissertation, The University of Michigan, 2001.

[34] Alex Christou and Manish Jugroot. Modeling of an electric propulsion system: Towards a hybrid system. *45th AIAA Plasmadynamics and Lasers Conference*, AIAA 2014-2233, 2014.

[35] Alex Christou and Manish Jugroot. Investigation of a micro ion thruster for microsatellites. *65th International Astronautical Congress*, IAC-14-C4.4.5, 2014.

[36] L. Garrigues, S. Mazouffre, and G. Bourgeois. Computed versus measured ion velocity distribution functions in a Hall effect thruster. *Journal of Applied Physics*, 111(11):113301, 2012.

[37] Daniel A. Herman and Alec D Gallimore. Discharge Chamber Plasma Structure of a 30-cm NSTAR-type Ion Engine. *Jet Propulsion*, AIAA 2004-3794, 2004.

[38] Y. Raitses, D. Staack, A. Smirnov, and N. J. Fisch. Space charge saturated sheath regime and electron temperature saturation in Hall thrusters. *Physics of Plasmas*, 12(7), 2005.

[39] I Maqueda, D Escobar, and E Ahedo. Advances on a Hall thruster hybrid code. *30th International Electric Propulsion Conference*, IEPC 2007-066, 2007.

[40] J Vaudolon, B Khiar, and S Mazouffre. Low and high frequency oscillations of the accelerating electric field in a Hall thruster. *33rd International Electric Propulsion Conference*, IEPC-2013-089, 2013.

[41] Richard Hofer, Ira Katz, Ioannis Mikellides, and Manuel Gamero-Castano. Heavy Particle Velocity and Electron Mobility Modeling in Hybrid-PIC Hall Thruster Simulations. *42nd AIAA/ASME/SAE/ASEE Joint Propulsion Conference & Exhibit*, AIAA 2006-4658, 2006.

[42] J. E. Polk, J. R. Anderson, J. R. Brophy, V. K. Rawlin, M. J. Patterson, J. Sovey, and J. Hamley. An Overview of the Results from an 8200 Hour Wear Test of the NSTAR Ion Thruster. *35th AIAA/ASME/SAE/ASEE Joint Propulsion Conference & Exhibit*, AIAA 99-2446, 1999.

[43] Ioannis G. Mikellides, Ira Katz, Richard Robert Hofer, Dan M. Goebel, Kristi De Grys, and Alex Mathers. Magnetic Shielding of the Acceleration Channel Walls in a Long-Life Hall Thruster. *46th AIAA/ASME/SAE/ASEE Joint Propulsion Conference & Exhibit*, AIAA 2010-6942, 2010.

[44] Trevor Morris, Cecile Malardier-Jugroot, and Manish Jugroot. Characterization of electrospray beams for micro-spacecraft electric propulsion applications. *Journal of Electrostatics*, 71:931–938, 2013.

[45] Tsuyohito Ito, Nicolas Gascon, W Crawford, and MA Cappelli. Further Development of a Micro Hall Thruster. *42nd AIAA/ASME/SAE/ASEE Joint Propulsion Conference*, AIAA 2006-4496, 2006.

[46] Guangye Chen and Laxminarayan L. Raja. Fluid modeling of electron heating in low-pressure, high-frequency capacitively coupled plasma discharges. *Journal of Applied Physics*, 96(11):6073, 2004.

Appendices

A Appendix A

A.1 Drift Diffusion Derivation

The electron flux shown in Equation 2.10 is derived from conservation of momentum. Beginning with Equation 2.6, momentum conservation may be simplified under a set of assumptions. Particularly, if ionization, attachment, and angular frequencies are less than the momentum transfer frequency, the first term on the left may be neglected.

$$\frac{\partial}{\partial t}(n_i m_i u_i) + \nabla \cdot n_i m_i \overrightarrow{u_i} \overrightarrow{u_i^T} = -(\nabla \cdot \underline{p_i}) + q_i n_i \overrightarrow{E} - n_i m_i \overrightarrow{u_e} \nu_m \tag{A.1}$$

Further, if the electron drift velocity is less than the thermal velocity, the second term on the left hand side may be neglected. For a Maxwellian electron distribution, the pressure term may be replaced by Equation A.2, where **I** is the identify matrix.

$$\underline{p_e} = n_e k_B T_e \underline{I} \tag{A.2}$$

The electron drift velocity may then be isolated as shown in Equation A.3.

$$\overrightarrow{u_e} = -\frac{k_B}{m_e \nu_m} \nabla T_e - \frac{k_B T_e}{n_e m_e \nu_m} \nabla n_e + \frac{q}{m_e \nu_m} \overrightarrow{E} \tag{A.3}$$

With the additional assumption that the condition in Equation A.4 holds, the electron flux as shown in Equation 2.10 can be defined.

$$\nabla T_e \ll \frac{T_e}{n_e} \nabla n_e \tag{A.4}$$

$$\overrightarrow{\Gamma_e} = -(\underline{\mu_e} \cdot \vec{E}) n_e - \overrightarrow{D_e} \cdot \nabla n_e \tag{A.5}$$

Where μ_e and D_e are defined in Equations A.6 and A.7 respectively.

$$\mu_e = \frac{q}{m_e \nu_e} \tag{A.6}$$

$$D_e = \frac{k_B T_e}{m_e \nu_e} \tag{A.7}$$

Further discussion of the drift-diffusion approximation may be found in Chen et al [46].